DOI: 10.26599/FSHW.2025.9250704

Contents lists available at SciOpen

Food Science and Human Wellness

journal homepage: https://www.sciopen.com/journal/2097-0765

China Food Publishing Co.

Hypolipidemic Effects of Yellow Wine Lees Protein and its Peptides: Extraction, Mechanism, and Functional Food Potential

Hongpeng Yu[1,2,*], Cansheng Ou[1,*], Dong He[1,2,#], Jinjin Yang[1], Kegang Wu[1,2], Zhengxiang Cui[1], Xianghua Chai[1,2], Yongqi Cheng[3], Wenhui Li[4], Xuejuan Duan[1], Chenghua Wang[5], Shengli Wang[6]

[1] *School of Chemical Engineering and Light Industry, Guangdong University of Technology, No. 100 Waihuan Xi Road, Panyu District, Guangzhou 510006, China*

[2] *Guangdong Provincial Laboratory of Chemistry and Fine Chemical Engineering Jieyang Center, Guangdong University of Technology, Jieyang City 522000, China*

[3] *Synergy Innovation Institute for Modern Industries, Guangdong University of Technology, Dongyuan 517500, China*

[4] *Heyuan Jinhuangtian Liquor Industry Co., Ltd, Heyuan City 517500，China*

[5] *College of Light Industry and Food Engineering, Guangxi University, Nanning, 530004, China*

[6] *Guangdong Baiweijia Taste Industry Technology Co., Ltd, Dongguan City, 523400, China*

ABSTRACT: Yellow wine lees, a by-product of Chinese yellow rice wine fermentation, are underutilized and pose environmental risks. This study extracted yellow wine lees protein (YWLP) using alkaline extraction and ultrasonic treatment, exploring its hypolipidemic activity and mechanism. YWLP exhibited antioxidant properties, pancreatic lipase (PL) and cholesterol esterase (ChE) inhibition, bile acid salt binding, and inhibition of cholesterol micellar solubilization. In a high-fat HepG2 cell model, YWLP (62.5-2000 μg/mL) significantly reduced ($P < 0.05$) intracellular lipid levels, aspartate aminotransferase (AST), alanine aminotransferase (ALT), total cholesterol (TC) and triglycerides (TG), while increasing high-density lipoprotein (HDL-C). Ultrafiltration revealed the < 3 kDa fraction as having the most significant lipid-lowering effect, while lipid-lowering peptides (SRGFGF, SWCRC, and FNLPR) were identified through LC-MS/MS and molecular docking. *In vitro* experiments confirmed the optimal lipid-lowering effect of SWCRC, with IC_{50} values of (1.153 ± 0.14) mmol/L for PL and (6.587 ± 0.228) mmol/L for ChE. Ultraviolet-visible spectroscopy, fluorescence spectroscopy, and molecular dynamics revealed its mechanism, confirming significant affinity toward both enzymes. Meanwhile, a *Caenorhabditis elegans* model was used to test lipid inhibition at different concentrations SWCRC (125-2000 μmol/L), and the results showed that lipids were significantly reduced in the SWCRC group compared with the model group ($P < 0.05$). These results suggest YWLP could serve as a natural lipid-lowering agent in functional foods, offering a sustainable use for yellow wine lees.

Keywords: Protein extracts; Yellow wine lees; Hypolipidemic activity; Bioactive peptides; Molecular docking; Inhibition mechanisms;

1. Introduction

#Corresponding author
hedong86284116@163.com
**These authors contributed equally to this work*

Received 27 March 2025
Received in revised from 23 April 2025
Accepted 12 May 2025

Chinese yellow wine, distinguished by its mellow taste, rich flavor, and distinctive red color [1]. Yellow wine is produced from glutinous and/or indica rice, which undergoes a series of processes including soaking, steaming, cooling, the addition of wine curds, fermentation, pressing, filtration, boiling, and storage [2]. The lengthy saccharification and fermentation process that produces yellow wine breaks down proteins and starches into amino acids, peptides, low molecular weight sugars, and other substances that can improve memory and prevent health problems such as thrombosis, coronary heart disease, and high blood pressure [3, 4]. Yellow wine lees, a residual by-product generated during the production of yellow rice wine, is recognized as a protein-rich resource (28.14% on a dry weight basis) [5] and serves as a valuable biomass material [6]. According to statistics, the production of yellow wine lees reached 0.3 to 0.4 million tons in 2020 [6], presenting significant potential for food applications due to its large volume and rich protein content. The development and utilization of yellow wine lees can not only provide an additional source of income for the yellow wine industry but also alleviate the environmental pollution caused by its disposal [7].

The prevalence of hyperlipidemia, a metabolic condition characterized by excessive levels of blood lipids or lipoproteins in plasma, has rapidly increased due to improvements in quality of life and substantial dietary changes [8], becoming a global public health issue. Thus, the prompt prevention and effective management of hyperlipidemia are paramount. The suppression of pancreatic lipase (PL) and cholesterol esterase (ChE), essential enzymes responsible for the breakdown of dietary triglycerides (TG) and cholesterol esters, respectively [9], has been linked to reduced fat absorption and bioavailability, leading to lipid-lowering effects [10]. Although synthetic drugs that effectively inhibit ChE and PL have been developed to treat hypercholesterolemia and obesity [11], their prolonged use may lead to adverse side effects on human health. As a result, the pursuit of safe and efficacious natural lipid-lowering agents has emerged as a critical focus in contemporary research.

According to two traditional Chinese medical texts, *Qí Mín Yào Shù* and *Běn Cǎo Gāng Mù*, drinking Hakka yellow rice wine over time is thought to assist control of blood pressure and glucose-lipid metabolism while also slowing down the aging process [2]. As a by-product of the yellow wine production process, yellow wine leaves present significant potential for exploitation due to their high nutritional value. The amino acid profile of rice protein in yellow wine lees closely aligns with the ideal dietary pattern recommended by the World Health Organization, offering potential health benefits [12]. To date, several novel bioactive peptides have been identified from Chinese yellow wine lees, including antioxidant peptides such as ALPHAIL, EWAPGAH, and FDDLYFDR [13], angiotensin I-converting enzyme inhibitory peptides including SNYFPRPW, WLGYPR, and DLRYW [5], as well as multifunctional peptides with both antioxidant and umami-enhancing properties, such as DPDGW and DNPNW [14]. However, to the best of our knowledge, no studies have yet reported the identification of lipid-lowering bioactive compounds derived from rice wine lees.

Food-derived bioactive peptides have attracted considerable attention due to their diverse biological activities, high safety profile, strong tissue affinity, and broad-spectrum effects, making them promising

candidates for development into pharmaceuticals or functional food products [15, 16]. These attributes make such peptides ideal natural and safer alternatives for the prevention and treatment of hyperlipidemia [17]. In recent years, numerous studies have demonstrated that bioactive peptides derived from various protein sources exhibit excellent lipid-lowering effects [18-21]. Therefore, the identification of hypolipidemic peptides from rice wine lees merits further in-depth investigation.

This study will extract yellow wine lees protein (YWLP) and evaluate their hypolipidemic activity by assessing their inhibitory effects on PL and ChE activities, bile acid salt binding capacity, cholesterol micelle formation, and HepG2 cell viability. The proteins will then be separated into peptides of varying molecular weights using ultrafiltration. Peptides exhibiting strong lipid-lowering activity will be identified through mass spectrometry and molecular docking. The lipid-lowering effects of these peptides will subsequently be validated through *in vitro* experiments and molecular dynamics simulations to elucidate the inhibition mechanism. And exploring the hypolipidemic effect of peptides *in vivo* through the C. *elegans* model. By elucidating the interaction mechanism between cells and molecules, this study established a basic framework for evaluating the hypolipidemic effect of yellow rice wine by-products, and provided a possibility for the development of biological activity and industrial transformation of yellow rice wine lees.

2. Materials and methods

2.1Materials and reagents

Hakka yellow rice wine lees were obtained from Jinhuangtian Liquor Co. Ltd. (Heyuan, Guangdong, China). 2,2'-Azinobis- (3-ethylbenzthiazoline-6- sulphonate) (ABTS), pyrogallol, vitamin C (Vc), 2,2-Diphenyl-1-picrylhydrazyl (DPPH), sodium cholate (SC), pancreatic lipase(PL), sodium taurocholate (STC), p-nitrophenyl laurate (p-NPL), cholesterol esterase(ChE), p-nitrophenyl butyrate (p-NPB), Nile red were purchased from Shanghai Macleans Biochemical Co., Ltd. (Shanghai, China); HepG2 cells, oil red O dye, hematoxylin dye, paraformaldehyde were purchased from Wuhan Bioqiandu Technology Co., Ltd. (Hubei, Wuhan, China); Peptide Synthesised by Nanjing Jiepeptide Biotechnology Co., Ltd. (Jiangsu, Nanjing, China); *Caenorhabditis elegans* (wild-type N2) and *Escherichia coli* (OP50) were purchased from Zhuhai Xinrui Trading Co., Ltd. (Zhuhai，Guangdong， China); All other chemicals and reagents used were of analytical grade.

2.2 Basic composition analysis of yellow wine lees

Protein levels were measured via the Kjeldahl method (GB 5009.5-2016). The fat content analysis employed Soxhlet extraction (GB 5009.6-2016), while enzymatic hydrolysis quantified starch composition (GB 5009.9-2016). Moisture evaluation utilized direct drying (GB 5009.3-2016), with ash quantification adhering to the national total ash protocol (GB 5009.4-2016). Crude fiber measurement implemented acid-alkali treatment (GB/T 5009.10-2003).

2.3 Protein extraction and electrophoresis

Protein extraction was performed using 200 g of dried wine lees powder mixed with 2 L of boric acid-potassium chloride buffer (pH 9.0). The mixture was first water bathed at 57℃ for 2 h, then subjected to ultrasound treatment (250 W, 30 min). After sequential filtration and centrifugation, the pH was adjusted to 4.0 with HCl. Protein precipitation was achieved through additional centrifugation (8,000 r/min, 15 min), followed by freeze-drying for storage.

Following the Solarbio kit instruction manual, a 15% separating gel and a 5% stacking gel were prepared for pre-electrophoresis. Various concentrations of YWLP solution were prepared, and 20 μL of 5× protein loading buffer was mixed with 80 μL of each protein sample. Mix well and boil for 10 min. Afterward, the prepared SDS-PAGE gels were properly loaded with 10 μL of each sample and subjected to electrophoresis for further analysis.

2.4 In vitro experiments to verify the lipid-lowering effect of YWLP

2.4.1 Antioxidant test of YWLP

The ABTS radical scavenging assay was modified from the method of Zhang et al. [22], with the ABTS working solution prepared following the method of Wang et al. [23]. Experimental procedures were performed in 96-well microplates by sequential addition of 100 μL YWLP (gradient concentrations) and 100 μL ABTS working solution. After incubation in dark conditions (ambient temperature, 5 min), absorbance values were recorded at 734 nm with a microplate reader (SuperMax 3100, Flash, China).

DPPH radical scavenging experiments were performed with a slight modification of the method described by Kumar et al. [24] and He et al. [25], an equal volume of 0.1 mmol/L DPPH was added to 100 μL of YWLP solution of different mass concentrations. After thorough mixing, the reaction systems were maintained under light-protected conditions for 30 min prior to measurement at 517 nm.

Superoxide anion scavenging activity was determined using an o-phenyltriol oxidation inhibition assay modified from Zhang et al. [26]. The experimental procedure involved sequential addition of 4.5 mL Tris-HCl buffer (pre-incubated at 25℃ for 20 min), 1 mL gradient-concentration YWLP samples, and 0.4 mL 25 mmol/L o-phenyltriol solution. The mixture was vortex-mixed and incubated at 25℃ for 5 min under light-protected conditions. Reaction termination was achieved by adding 1 mL 8 mmol/L HCl, followed by immediate absorbance measurement at 299 nm.

The blank and positive controls were Tris-HCl and vitamin C (Vc), respectively. The ABTS, DPPH or superoxide anion (O_2^-) scavenging rate was determined using the subsequent formula.

$$\text{ABTS, DPPH or } O_2^- \text{ scavenging rate}(\%) = \left(1 - \frac{A_1 - A_2}{A_3 - A_4}\right) \times 100 \quad (1)$$

A_1 indicates the absorbance value of the experimental group, A_2 signifies the absorbance value of the sample background group, A_3 reflects the absorbance value of the no-sample control group, and A_4 represents the absorbance value of the control background group.

2.4.2 Evaluation of PL and ChE inhibitory activity of YWLP

Minor modifications were made based on the method described by Lu et al. [27]. Involved sequential mixing of 50 μL gradient-concentration samples (0.03125-2.0 mg/mL) with 50 μL 1.0 mg/mL PL solution, followed by incubation (37℃, 10 min). The reaction system was then supplemented with 100 μL 2.0 mmol/L p-NPL solution and subjected to secondary incubation (37℃, 30 min). Absorbance values were quantified at 405 nm using a enzyme marker (SuperMax 3100, Flash, China).

ChE inhibitory activity was evaluated using the method described by Huang et al. [28], with minor modifications. The reaction commenced by combining 50 μL of protein solution at differing concentrations (0.03125-2.0mg/mL) with 100 μL of PBS (0.01M, pH 7.4) that included 5.16 mmol/L sodium taurocholate and 5 mmol/L p-NPB. Fifty microliters of 0.163 U/mL ChE was included into this mixture. Following a 15 min incubation at 37℃, the absorbance was measured at 405 nm.

Buffer served as the blank control, whereas orlistat functioned as the positive control. The inhibition rates for PL and ChE activities were determined using the subsequent formula.

$$\text{PL or ChE Inhibition rate (\%)} = \left(1 - \frac{A_3 - A_4}{A_1 - A_2}\right) \times 100 \quad (2)$$

A_1, A_2, A_3, and A_4 represent the absorbance values of enzyme + substrate, buffer + substrate, enzyme + sample + substrate, and sample + substrate in the reaction system.

2.4.3 PL and ChE activity inhibition type assay

The response rates of PL and ChE in the presence of inhibitors were assessed by diluting YWLP, PL, and ChE at various concentrations. OD values were recorded every minute for 10 min. The slopes of the time-OD curves represented the reaction rates of tryptic PL and ChE in the presence of the samples. A linear graph depicting enzyme reaction rates (OD/min) at different sample concentrations was created to analyze the type of inhibition of tryptic PL and ChE by YWLP.

2.4.4 Measurement of the bile acid salt binding ratio

The *in vitro* bile acid binding assay was conducted according to Hu et al. [29] with procedural adjustments. Mixing 3 mL of gradient-concentration samples with 3 mL pepsin solution (10 mg/mL) and 1 mL 10 mmol/L HCl, followed by incubation at 37℃ for 60 min. pH adjustment to 6.3 and addition of 4 mL trypsin solution (10 mg/mL) for secondary incubation (37℃, 60 min). Supplementation with 4 mL sodium taurocholate (0.5 mmol/L) and third incubation (37℃, 60 min). Centrifugation (4,000 r/min, 15 min) of the mixture, with supernatant treatment using 5 mL 60% sulfuric acid under thermal processing (70℃, 30 min, then, ice bath, 5 min). Absorbance was measured at 387 nm. The binding rate of sodium cholate (SC) was assessed at a concentration of 0.4 mmol/L. For the background group, no bile salts were included, but the procedure remained the same. The binding rate was determined using the subsequent formula.

$$\text{Binding rate}(\%) = \left(1 - \frac{A_1}{A_2}\right) \times 100 \quad (3)$$

A_1 is the amount of sodium cholate remaining and A_2 is the amount of sodium cholate added

2.4.5 Cholesterol micelle

The cholesterol micellar solution was produced according to the procedure outlined by Sun et al. [30], with minor changes. A phosphate-buffered saline (15 mmol/L, pH 7.4) containing 2 mmol/L cholesterol, 10 mmol/L sodium taurocholate, 132 mmol/L NaCl, and 5 mmol/L oleic acid was prepared and homogenized by ultrasonication. After 12 h incubation at 37℃, test samples (0.1875-6 mg) were dissolved in 3 mL of the micellar solution. The mixture was incubated at 37℃ with constant shaking for 2 h, followed by centrifugation at 12,000 r/min for 20 min. The supernatant was analyzed for cholesterol content using a total cholesterol (TC) kit, with the micellar solubility inhibition rate calculated according to the established formula.

$$\text{Cholesterol micelle solubility inhibition rate}(\%) = \left(1 - \frac{A_1}{A_2}\right) \times 100 \quad (4)$$

A_1 is the absorbance value of the blank group; A_2 is the absorbance value of the sample group;

2.5 Cellular experiments to verify the lipid-lowering effect of YWLP

2.5.1 Cell culture

HepG2 cells were maintained in DMEM supplemented with 10% fetal bovine serum and 1% streptomycin-penicillin under standard culture conditions (37℃, 5% CO_2, 95% humidity). The cells reached an optimal condition and were prepared for the subsequent experiments.

2.5.2 Cell proliferation toxicity

A modified variant of the CCK8 method was utilized to evaluate cytotoxicity levels in cells [22]. HepG2 cells in the logarithmic growth phase were enzymatically digested with trypsin and subsequently produced as a cell suspension. The cells were subsequently inoculated onto 96-well plates at a density of 6000 cells per well, with three replicate wells for each group, and incubated for 24 h. The cells were dosed separately for each group and incubated for another 24 h. The culture medium was replaced with 100 μL fresh DMEM containing 10% CCK-8 reagent. After 2 h incubation under light-protected conditions, absorbance was measured at 450 nm using a microplate reader (SuperMax 3100, Flash, China).

$$\text{Cell viability}\ (\%) = \left(1 - \frac{A_1 - A_0}{A_2 - A_0}\right) \times 100 \quad (5)$$

A_0 represents the absorbance of the blank control, A_1 denotes the absorbance of the experimental group, and A_2 signifies the absorbance of the negative control.

2.5.3 Induction of lipid accumulation in HepG2 cells

With slight modifications to the experimental method described by Shuai et al. [23], oleic acid was used as a model lipid source to induce excessive lipid accumulation in HepG2 cells. Log-phase HepG2 cells were seeded and cultured under the aforementioned conditions for 24 h. The culture medium was then replaced, and the cells were treated with 500 μmol/L oleic acid to induce lipid overload. Subsequently, different concentrations of YWLP were added, and the cells were incubated under the same conditions for another 24 h. Orlistat (20 μg/mL) was used as a positive control.

2.5.4 Cellular oil red O assay

HepG2 cell oil red O assay according to the method of He et al. [24], a control group, a model group, an orlistat group (20μg/mL), and a YWLP group were set up. Cellular fixation was performed using 4% paraformaldehyde (15 min). The cells were stained with oil red O for 1 to 2 h, then briefly washed with 60% isopropanol solution for 10 to 20 s. Finally, images were captured and analyzed under a microscope. Quantification was performed using ImageJ software.

2.5.5 Determination of the effect of YWLP on intracellular AST, ALT, HDL-C, TC, and TG content

Design the experiment with the same cell model group as the Oil Red O experiment. Following 24 h of incubation with YWLP, the cells were subjected to trypsin digestion for 3 to 5 min, and the resultant precipitate was collected using centrifugation. The cells were then lysed by ultrasonication in an ice-water. The activities of aspartate aminotransferase (AST), alanine aminotransferase (ALT), total cholesterol (TC), triglycerides (TG), and high-density lipoprotein (HDL-C) were assessed utilizing commercial kits in accordance with the guidelines.

2.6 Investigating the effects of different molecular weights of YWLP on PL and ChE activities

The samples were dissolved to the appropriate concentration and filtered through 0.22 μm aqueous filter membranes. They were separated into four fractions: < 3 kDa, 3-10 kDa, 10-30 kDa, and >30 kDa, using tubular membrane ultrafiltration equipment (Millipore, Darmstadt, Germany). The fractions were gathered and freeze-dried. Finally, PL and ChE inhibitory activities were assessed as described in section 2.4.2.

2.7 Identification of peptide sequences using LC-MS/MS

Slightly modified from the experimental method of Yang et al.[5], peptides were identified using an LC-MS/MS system (Easy-nLC 1200/QExactive, Thermo Fisher Scientific, USA). Liquid chromatography conditions included a 100 μm i.d. × 180 mm analytical column packed with Reprosil-Pur 120 C18 AQ 3 μm. The mobile phase system comprised 0.1% aqueous formic acid (phase A) and 80% acetonitrile/0.1% formic acid (phase B), delivered at 600 nL/min over a 66-min gradient: 0-55 min linear increase from 0% to 40% B, followed by 95% B isocratic elution (56-66 min). Mass spectrometric detection employed a data-dependent acquisition mode with full scans (100-1500 m/z) at 70,000 resolution (AGC target 3e6, MaxIT 100 ms), triggering top-20 precursor ions for HCD fragmentation (28% NCE) analyzed at 17,500 resolution (AGC 1e5, MaxIT 50 ms). MS/MS data were processed using software to match the collected data with the theoretical peptide fragments.

2.8 Molecular Docking

Peptide bioactivity was assessed with PeptideRanker (https://distilldeep.ucd.ie/PeptideRanker/), with peptides scoring > 0.8 categorized as active peptides. Molecular docking was conducted with Discovery Studio 2019 (DS2019) software. The three-dimensional conformation of the peptide was developed from the amino acid sequence of the bioactive peptide, and molecular docking was performed using PL (PDB number: 1LPB) and ChE (PDB ID: 1AQL), both sourced from the RCSB Protein Data Bank (http://www.rcsb.org). Key amino acids selected for docking included Phe77, Ser152, Asp176 and His263

for PL, Ser194, Asp320 and His435 for ChE. The initial screening used LibDock semi-flexible molecular docking to select peptides with a LibDock Score greater than 150. Subsequently, flexible docking was performed and the results were evaluated and visualised using DS2019. DS2019 was employed to visualize the docking results in both 2D and 3D to assess the docking interactions and binding affinities.

2.9 In vitro validation of the hypolipidemic effect of synthetic peptides

2.9.1 Inhibition studies of PL and ChE activity by synthetic peptides

The inhibitory efficacy of the synthesized peptides against PL and ChE was assessed utilizing the methodology outlined in section 2.4.2. In the PL experiment, PBS (0.01 M, pH 7.4) substituted Tris-HCl.

The reversibility of enzyme activity was analyzed experimentally with reference to 2.4.3. The reversibility of SWCRC-induced PL and ChE inhibition was analyzed by varying the enzyme concentration. By making minor adjustments to the experimental approach of Shen et al. [31], the inhibitory mechanism of PL and ChE by SWCRC was clarified by a Lineweaver-Burk plot, illustrating the reciprocal of the SWCRC concentration against the reciprocal of the reaction rate. Absorbance was measured every 30 s for 10 min at 405 nm using an enzyme marker (SuperMax 3100, Falsh, China). The type of PL and ChE inhibition by SWCRC was determined using the Lineweaver-Burk equation:

$$\frac{1}{V} = \frac{K_m + S}{V_{max}S} = \frac{K_m}{V_{max}} \times \frac{1}{S} + \frac{1}{V_{max}} \tag{6}$$

V, V_{max}, K_m, and S denote the enzyme velocity, maximal enzyme velocity, Michaelis-Menten constant, and substrate concentration in the presence and absence of SWCRC, respectively.

2.9.2 Ultraviolet-visible and fluorescence spectroscopy

Experiments in Ultraviolet-visible (UV-visible) spectrometry and fluorescence spectrometry were conducted following the methodology of Huang et al.[32]. The UV-visible absorption spectra of PL (2 mg/mL), ChE (0.326 U/mL), and mixtures with varying concentrations of SWCRC were recorded using a UV-visible spectrophotometer (TU-1950, PERSEE, China). Absorption scans were conducted over the range of 200 - 500 nm.

Fluorescence spectra were analyzed using an enzyme marker (Varioskan LUX, Thermo Scientific, Finland), with the excitation wavelength established at 280 nm. Emission spectra were obtained from 300 - 500 nm at 37°C, utilizing a slit width of 5 nm. The evaluation of fluorescence quenching was conducted using the Stern-Volmer equation.

$$\frac{F_0}{F} = K_{SV}[Q] + 1 = K_q\tau_0[Q] + 1 \tag{7}$$

$$lg\frac{(F_0 - F)}{F} = lgK_a + nlg[Q] \tag{8}$$

F and F_0 represent the fluorescence intensities in the presence and absence of the inhibitor, respectively; K_{SV} is the Stern-Volmer quenching constant; K_q is the quenching constant; K_a is the binding constant; [Q] denotes the concentration of the quencher; n is the number of binding sites; and τ_0 is the average fluorescence lifetime of the substance in the absence of a quencher, typically 1×10^{-8} s for biomolecules.

2.10 Molecular dynamics (MD) simulation

The conformational stability of the SWCRC-PL/ChE complex was assessed through 100-ns molecular dynamics simulations performed using GROMACS (v2020.6) with AMBER 99SB force field, based on the molecular docking results. The test system was set up in a cubic box and filled with water molecules to mimic a solution environment, while Na^+ and Cl^- ions were added to neutralize the system's total charge. The system underwent energy minimization using the steepest descent method, followed by equilibrium simulations under NVT (298.15 K) and NPT (1.0 bar) conditions. Finally, unconstrained productive MD simulations were performed on the equilibrated system, and the root mean square deviation (RMSD), root mean square fluctuation (RMSF), and radius of gyration (Rg) were calculated using the analytical tools in GROMACS to assess the system's dynamic behavior and stability.

2.11 In vivo validation experiments of the hypolipidemic effect of SWCRC

2.11.1 Culture of Caenorhabditis elegans

With slight modifications to the method described by Zhang et al.[21], adult *Caenorhabditis elegans* (C. *elegans*) were treated with a lysis solution (1 M NaOH, 5% NaClO) to obtain synchronized L1 larvae. The larvae were then inoculated onto nematode growth medium (NGM) plates seeded with Escherichia coli OP50 and incubated at a constant temperature of 20℃ for 48 h until reaching the L4 stage. Subsequently, the C. *elegans* were transferred to NGM plates containing 12.5 μg/mL 5-fluoro-2'-deoxyuridine (control group), as well as NGM plates supplemented with various concentrations of SWCRC (0-2000 μmol/L) or the orlistat (50 μmol/L) in the presence of 2% glucose and 12.5 μg/mL 5-fluoro-2'-deoxyuridine. The C. *elegans* were then cultured for an additional six days for further analysis.

2.11.2 Escherichia coli OP50 bacterial growth assay

With slight modifications to the method described by Lin et al.[33], 10 μL of *Escherichia coli* (*E. coli*) OP50 bacterial suspension (OD_{600} = 0.4) was added to 1 mL of LB medium containing SWCRC at final concentrations of 0, 125, 250, 500, 1000, and 2000 μmol/L. Incubate at 37° C for 12 h and measure absorbance at 600 nm at 2 h intervals.

2.11.3 Oil Red O and Nile Red Colouring

With slight modifications to the method described by Zhang et al.[21], the stock solution of Oil Red O (5 mg/mL in isopropanol) was diluted with distilled water at an isopropanol-to-water ratio of 3:2. The solution was then filtered through a 0.22 μm membrane and left to stand in the dark for 12 h to prepare the Oil Red O working solution. C. *elegans* were washed three times with M9 buffer, followed by fixation in 60% isopropanol at room temperature for 5 min. After centrifugation and removal of the supernatant, the worms were incubated with the Oil Red O staining solution in the dark for 2 h. After staining, the worms were rinsed with M9 buffer, and images of red lipid distribution were captured using an inverted fluorescence microscope (MF53-N, Mshot, China).

The fixation and staining procedure for the Nile Red assay followed the same protocol as the Oil Red O staining. C. elegans were incubated in a 0.003 μg/mL Nile Red working solution, and lipid droplet signals were captured using a high-resolution laser confocal microscope (LSM 800 with Airyscan, Zeiss, Germany).

The stained area and lipid droplet area were analyzed using ImageJ software to quantitatively compare lipid content and droplet distribution across different groups.

2.11.4 Determination of TG

With slight modifications based on the method of Bai et al.[34], approximately 1,000 C. *elegans* were collected and lysed in a buffer containing protease inhibitors. The samples were then subjected to ultrasonication on ice, followed by centrifugation at 12,000 r/min for 10 minutes to collect the supernatant. TG content was measured using a TG assay kit (Beyotime, Shanghai, China) according to the manufacturer's instructions. Protein concentration was determined using a BCA assay kit (Biosharp, Anhui, China). The TG content was normalized to the protein concentration.

2.12 Statistical analysis

All the experiments were repeated three times. Data were examined via one-way analysis of variance (ANOVA) with IBM SPSS version 27.0 software. The level of statistical significance was set at $P < 0.05$.

3. Results

3.1 Protein basic composition and electrophoresis analysis

To further investigate the active components in yellow wine lees, this study conducted a compositional analysis of yellow wine lees that had not undergone water filtration and non-dried, as shown in Table S1. The results indicate that the wet yellow wine lees primarily consist of water, with a moisture content reaching 93.1%. Proteins account for 3.52%, while the starch content is 2.38%. The total proportion of ash, fat, and crude fiber is less than 1%. Compositional analysis revealed that the fresh yellow wine lees, due to the lack of drying, were predominantly composed of water. However, after removing the 93.1% water content, it was found that proteins accounted for the highest proportion, reaching 51.0%. This indicates that the dry basis of yellow wine lees is extremely rich in proteins and polysaccharides.

Proteins extracted from yellow wine lees were analyzed by SDS-PAGE to determine their molecular weight distribution. The electrophoretic profiles of YWLP at different concentrations are shown in Fig. 1(a). The results indicate that the majority of the protein components are below 25 kDa, with distinct bands also observed below 15 kDa. These results suggest that the alkali extraction process effectively yielded YWLP with relatively low molecular weights.

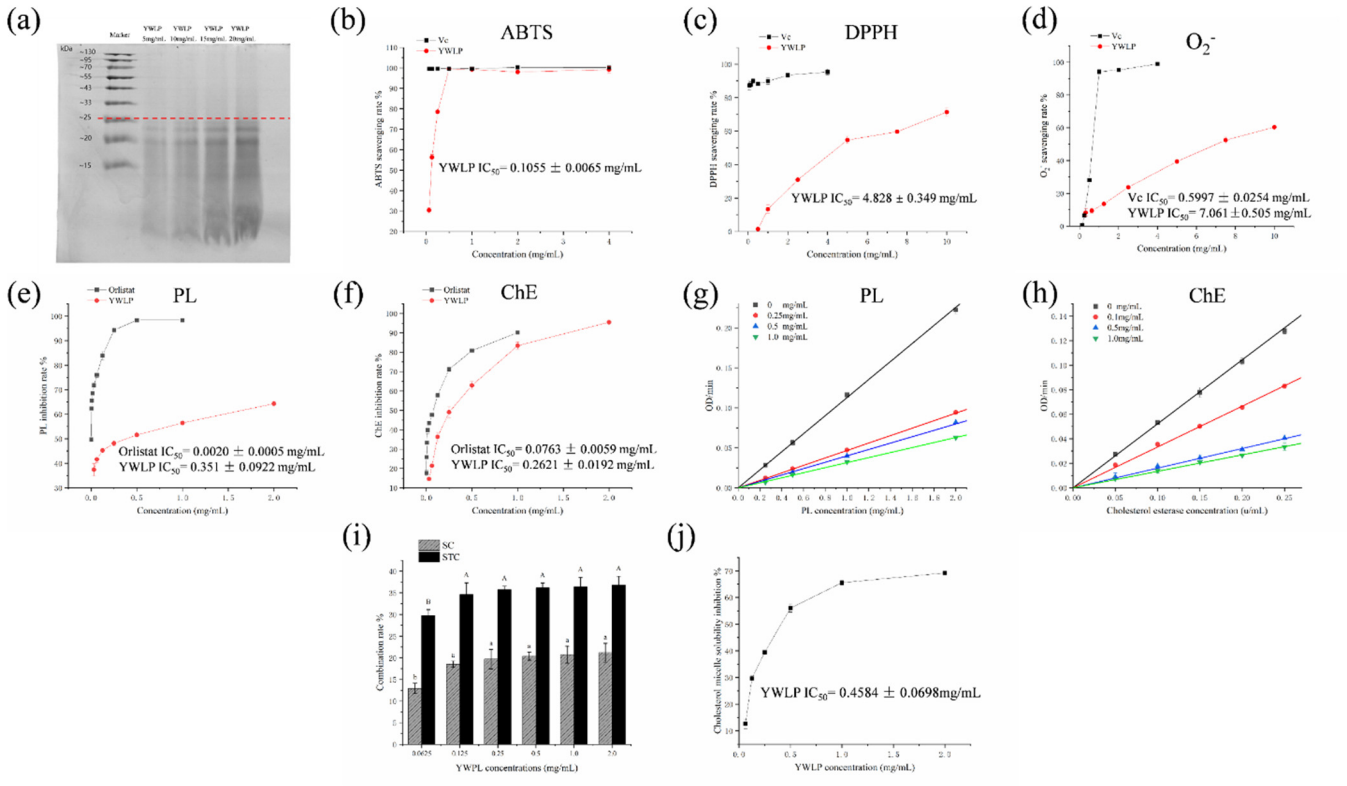

Fig. 1 *In vitro* lipid-lowering effects of YWLP. (a) SDS-PAGE of YWLP at varying concentrations; (b-d) ABTS, DPPH, and O_2^- radical scavenging activities; (e-f) Inhibitory effects on PL and ChE; (g-h) Kinetics of YWLP inhibition on PL and ChE; (i) Cholate-binding capacity; (j) Cholesterol micelle solubility. Different letters denote significant differences ($P < 0.05$).

3.2 Analysis of the results of YWLP in vitro experiments

To investigate the potential antioxidant properties of YWLP, this study employed Vc as a positive control and evaluated the ability of YWLP to scavenge ABTS radicals, DPPH radicals, and O_2^- radicals. The radical scavenging activities of YWLP toward ABTS, DPPH, and O_2^- are illustrated in Fig. 1 (b-d). The results demonstrated that YWLP exhibited the strongest scavenging activity against ABTS radicals, followed by DPPH radicals, and the weakest activity was observed against O_2^- radicals. Nevertheless, YWLP showed scavenging effects against all three types of radicals. The IC_{50} values of YWLP for ABTS, DPPH, and O_2^- radicals were (0.1055 ± 0.0065) mg/mL, (4.828 ± 0.349) mg/mL, and (7.061 ± 0.505) mg/mL, respectively. These findings indicate that YWLP possesses notable antioxidant activity, suggesting its potential as a bioactive compound.

To verify our hypothesis regarding the hypolipidemic effect of YWLP, this study investigated the inhibitory activity and reversibility of YWLP against PL and ChE, its bile acid-binding capacity, and its ability to suppress cholesterol micelle solubility. As shown in Fig. 1(e-f), YWLP exhibited notable inhibitory effects on both enzymes. The inhibition rates of PL and ChE increased in a concentration-dependent manner. The IC_{50} values for PL and ChE were (0.351 ± 0.0922) mg/mL and (0.2621 ± 0.0192) mg/mL, respectively. At a protein concentration of 2 mg/mL, the inhibition rates reached (64.32 ± 1.06)% for PL and (95.53 ± 0.39)% for ChE. YWLP showed a notable inhibition effect on both enzymes.

Fig. 1(g-h) illustrate the reversibility of the enzyme inhibition by YWLP. Enzyme kinetics analysis was conducted to determine the inhibition type of YWLP on PL and ChE. The relationship between PL concentration and reaction rate exhibited a linear pattern, with all lines passing through the origin. As the concentration of YWLP increased, the slope of the fitted equation decreased. Similarly, the kinetic results for ChE were consistent with those of PL: all lines passed through the origin, and the slopes of the fitted equations decreased with increasing YWLP concentrations. These findings suggest that YWLP did not irreversibly inactivate PL and ChE but rather reduced their catalytic activity. YWLP inhibits PL and ChE reversibly by binding through non-covalent interactions.

The investigation of bile salt-binding capacity offers theoretical insight into the lipid-lowering mechanisms of functional substances. Fig. 1(i) illustrates the bile salt-binding efficacy of YWLP. This study found that at a protein concentration of 0.0625 mg/mL, there were significant differences ($P < 0.05$) in binding capacity for both SC and STC compared to other concentrations. When the protein concentration reached 0.125 mg/mL, the binding capacities of SC and STC were (18.54 ± 0.72)% and (34.63 ± 2.69)%, respectively. However, when the concentration exceeded 0.25 mg/mL, further increases did not lead to significant improvements in bile salt binding, and only a weak positive correlation between concentration and binding rate was observed. Nonetheless, YWLP exhibited a certain degree of bile salt-binding ability and was capable of interacting with bile salts at relatively low concentrations, thereby supporting its potential lipid-lowering efficacy.

Effective inhibition of cholesterol micelle solubility plays a positive role in controlling blood lipid levels. As shown in Fig. 1(j), the inhibitory rate of YWLP on cholesterol micelle solubility increased steadily with concentrations ranging from 0.0625 to 2.0 mg/mL. The IC_{50} value for this inhibition was determined to be (0.4584 ± 0.0698)mg/mL. At a YWLP concentration of 2.0 mg/mL, the inhibition rate reached (69.20 ± 0.23)%. These results suggest that YWLP has the potential to serve as a natural candidate for cholesterol-lowering applications.

In summary, YWLP exhibited strong inhibitory activity against PL and ChE, with evidence supporting reversible enzyme inhibition. Additionally, YWLP demonstrated measurable bile salt-binding capacity and effectively reduced the solubility of cholesterol micelles. These findings support its potential as a natural lipid-lowering agent and justify further investigation into its active peptide components.

3.3 Hypolipidemic effect of YWLP on HepG2 cell assay

To further elucidate the lipid-lowering potential of YWLP, experiments were conducted using HepG2 cells. First, the cytotoxicity of YWLP was assessed by measuring the viability of HepG2 cells using the CCK-8 assay, as shown in Fig. 2(a). YWLP was found to reduce cell viability in a dose-dependent manner. At concentrations of 500 μg/mL and below, cell viability remained above 90%, whereas at 2000 μg/mL, the survival rate decreased to (55.75 ± 1.09)%, indicating cytotoxicity at high doses.

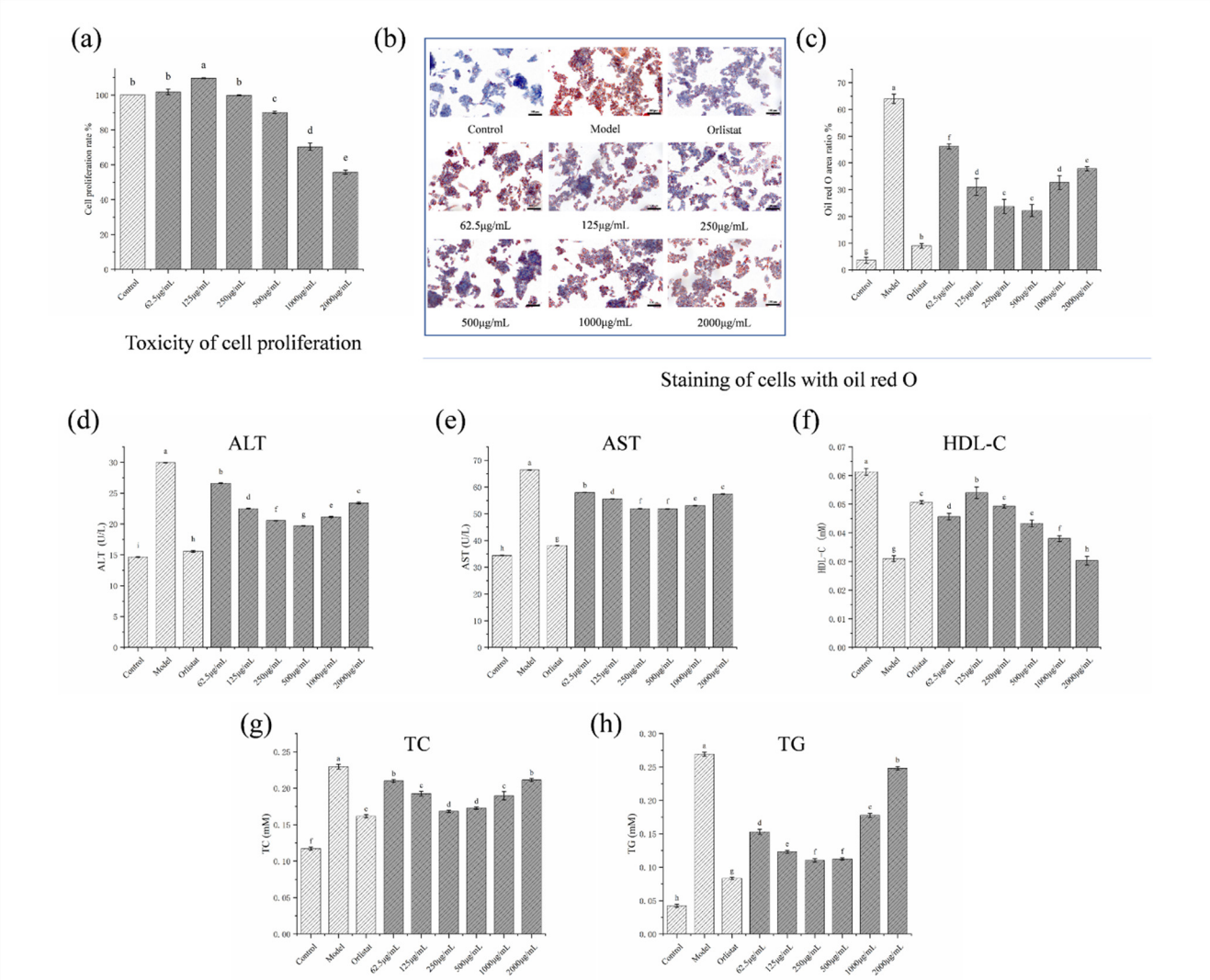

Fig. 2 Lipid-lowering effect of YWLP on HepG2 cells. (a) Cytotoxicity analysis at varying YWLP concentrations; (b) Oil Red O staining of cells; (c) Quantification of lipid accumulation from Oil Red O assay; (d-h) Effects on intracellular ALT, AST HDL-C, TC, and TG levels. Different letters indicate significant differences ($P < 0.05$).

Next, the inhibitory effect of YWLP on lipid accumulation was investigated using a HepG2 steatosis model. In Fig. 2(b), oil red O staining revealed distinct differences in lipid deposition among experimental groups. The control group showed minimal lipid accumulation (red area: (3.6 ± 1.1)%), while the model group exhibited extensive lipid droplet formation (red area: (64.0 ± 1.7)%), confirming successful induction of steatosis. As shown in Fig. 2(c), YWLP treatment significantly reduced lipid accumulation in HepG2 cells. Treatment with YWLP at concentrations of 62.5-500 μg/mL led to a decrease in intracellular lipid content. However, reductions in red-stained area at 250 μg/mL and 500 μg/mL were not statistically significant. At higher concentrations, the red staining area increased, which was consistent with the cytotoxic effects observed in the cell viability assay.

To gain deeper insights into the intracellular lipid-lowering effects of YWLP, HepG2 cell experiments were performed to evaluate its impact on intracellular levels of AST, ALT, HDL-C, TC, and TG, as presented in Fig. 2(d-h). The results showed that YWLP exerted beneficial effects on all measured indicators. Treatment with different concentrations of YWLP revealed that the most pronounced effects

occurred within the 250-500 μg/mL range, which may be partially influenced by the compound's cytotoxicity at higher concentrations. YWLP at concentrations between 62.5 and 500 μg/mL gradually reduced intracellular ALT and AST levels. However, both indicators began to increase when the concentration exceeded 500 μg/mL. The strongest effect on AST reduction was observed at 500 μg/mL, although the difference between 250 μg/mL and 500 μg/mL was not statistically significant. TG content reached its lowest value at 250 μg/mL (0.1103 ± 0.0025) mmol/L, representing a 59.0% decrease compared to the model group (0.269 ± 0.03) mmol/L. Similarly, TC also decreased to its lowest level at 250 μg/mL. The HDL-C level peaked at 125 μg/mL, surpassing that of the positive control group. Overall, YWLP significantly ($P < 0.05$) reduced intracellular AST, ALT, TC, and TG levels and enhanced HDL-C levels at all tested concentrations compared to the model group. Notably, the most effective results were observed at the lower concentration of 250 μg/mL, suggesting it as the optimal dose for intracellular lipid regulation.

In conclusion, YWLP significantly reduced lipid accumulation in HepG2 cells and modulated key biochemical indicators. Both *in vitro* and cellular experiments confirmed the lipid-lowering efficacy of YWLP and provided cellular-level evidence supporting its regulatory role in lipid metabolism.

3.4Hypolipidemic effects of YWLP with different molecular weights

Based on the confirmed inhibitory effects of YWLP in both in vitro and in vivo experiments, further investigation focused on evaluating the lipid-lowering activity of YWLP fractions with different molecular weights using ultrafiltration. As illustrated in Fig. 3, the fraction of YWLP with a molecular weight less than 3 kDa exhibited the strongest enzyme inhibitory activity. Compared with the 3-10 kDa, 10-30 kDa, and > 30 kDa fractions, the < 3 kDa peptide fraction demonstrated the most potent inhibitory effects on both PL and ChE at the same concentration. Therefore, subsequent experiments focused primarily on the < 3 kDa fraction due to its superior enzyme-inhibitory activity.

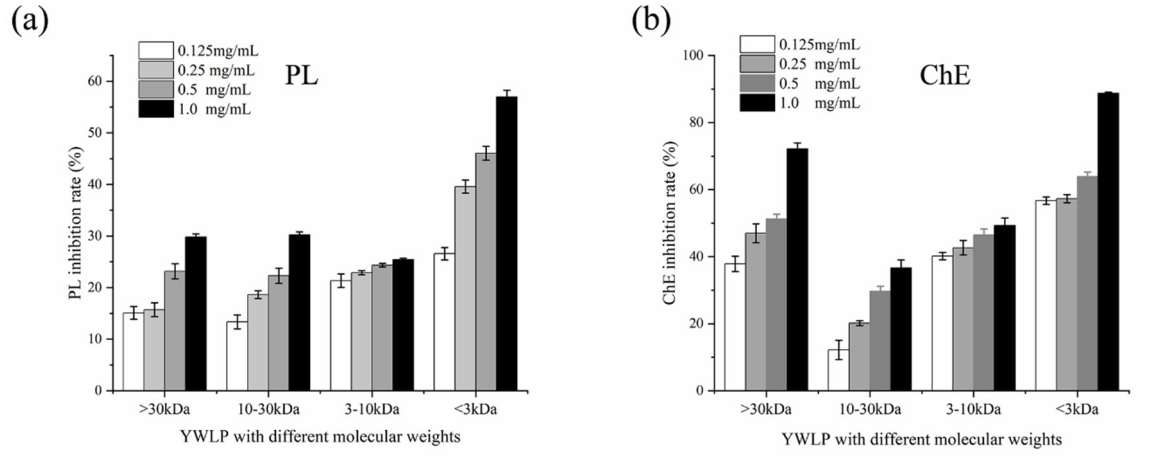

Fig. 3 Inhibitory effects of YWLP with different molecular weights on lipid-related enzymes. (a) Inhibition of PL; (b) Inhibition of ChE.

3.5 Identification of yellow wine lees peptides by mass spectrometry

LC-MS/MS analysis of the most active lipid-lowering YWLP fraction (< 3 kDa) identified 3,880 distinct peptide sequences, as shown in Fig. 4. Fig. 4(a-b) reveal that the peptides were predominantly of

low molecular weight and short chain length. Notably, peptides with molecular weights < 1 kDa accounted for the largest proportion—1,983 sequences, or 51.11% of the total—with tetrapeptides being the most abundant. A gradual decline in peptide count was observed with increasing peptide length. Fig. 4(c) presents the amino acid composition of the < 3 kDa peptides, indicating glycine (G) as the most abundant residue (7.98%), followed by arginine (R), alanine (A), valine (V), and leucine (L), each comprising more than 7% of the total amino acid content. Further analysis of peptide characteristics is illustrated in Fig. 4(d), which highlights the distribution of isoelectric points (pI) and grand average of hydropathicity (GRAVY). Most peptides exhibited pI values between 4 and 7, indicating a tendency toward weak acidity to near-neutrality. In addition, the GRAVY scores were mostly distributed between -0.5-0.5, suggesting a balanced composition of hydrophobic and hydrophilic residues. These physicochemical features imply favorable structural stability and solubility, which may enhance the bioactivity of the peptides.

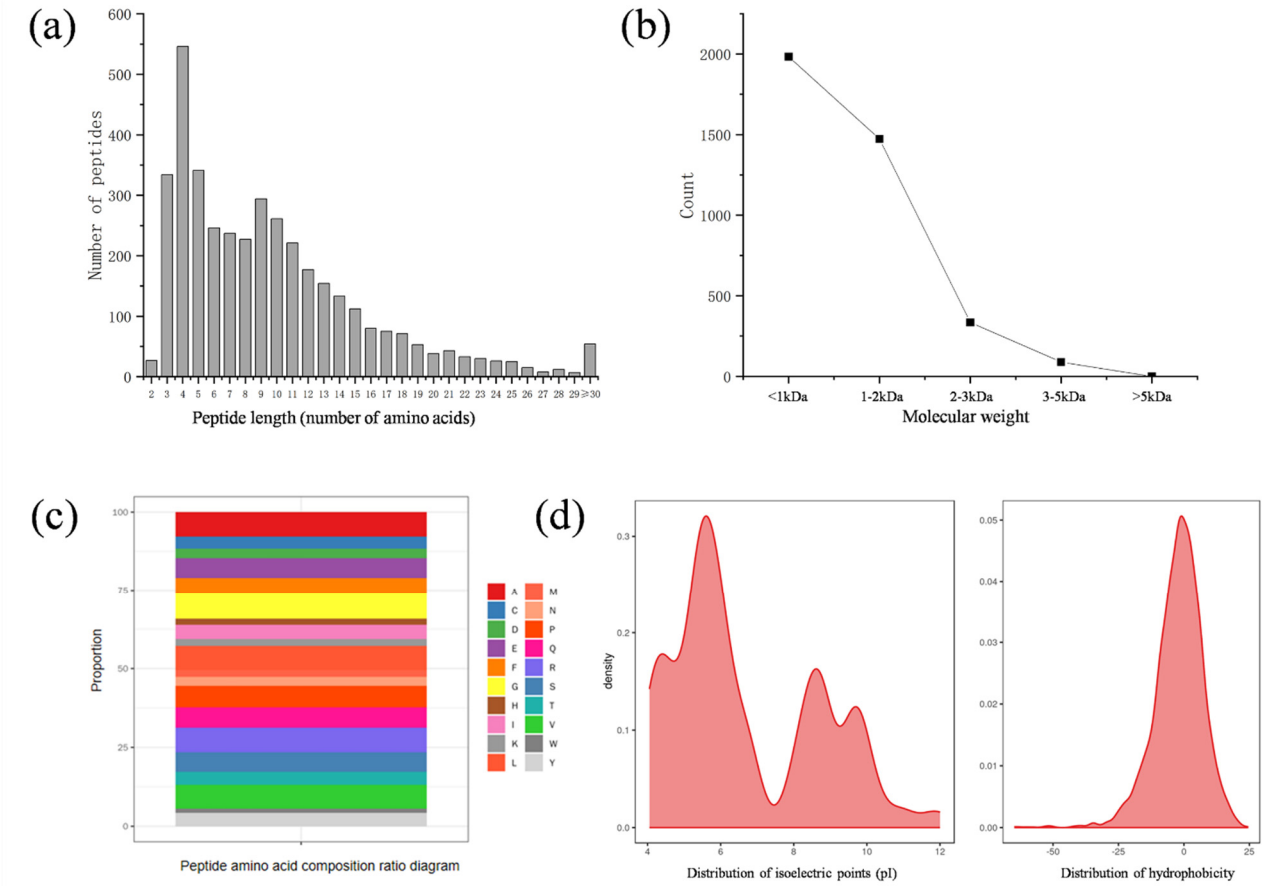

Fig. 4 LC-MS/MS analysis of < 3 kDa yellow wine lees-derived peptides. (a) Peptide length distribution; (b) Peptide abundance across molecular weight intervals; (c) Amino acid composition profile; (d) Isoelectric point and hydrophobicity distribution.

3.6 Molecular docking results

To identify the most potent lipid-lowering peptides from those obtained via LC-MS/MS analysis, bioactivity prediction was first conducted using PeptideRanker for peptides < 3 kDa. A total of 365 peptides were predicted to be bioactive with scores >0.8. These high-score peptides were then subjected to molecular docking using the LibDock module in Discovery Studio 2019 (DS2019). As a result, 281 peptides were successfully docked with PL, and 252 peptides were successfully docked with ChE. Among them, 12

peptides demonstrated strong dual-binding affinity to both enzymes, each with a co-LibDock score >160. These peptides were: SRGFGF, IHFQF, YAPWCGH, FNLPR, WLSYP, YVPW, SWCRC, SPFW, PTFPGCP, SWCR, FTFRP, and FCTMR. Subsequently, full flexible docking was performed on these 12 candidate peptides using the Flexible Docking module in DS2019. Three peptides (SRGFGF, SWCRC, and FNLPR) were identified as the most promising candidates based on their superior docking parameters, including PeptideRanker scores >0.8. LibDock scores >160, CDOCKER energy values >70 kcal/mol, CDOCKER interaction energy >60 kcal/mol, and binding energy values < -180 kcal/mol, as summarized in Table 1. Further analysis of the interaction modes between the three peptides and the two enzymes was performed using DS2019, and the results are presented in Fig. 5. These analyses revealed that SRGFGF, SWCRC, and FNLPR predominantly interacted with the active sites of PL and ChE through hydrogen bonding, alkyl, Pi-alkyl, and Pi-cation.

Table 1 Docking results of three peptides screened from yellow wine lees using molecular docking

Enzyme	Peptides	PeptideRanker Score	LibDock Score	-CDOCKER ENERGY (kcal/mol)	-CDOCKER INTERACTION ENERGY (kcal/mol)	Binding Energy (kcal/mol)
1LPB	SRGFGF	0.96031	181.009	97.9225	72.366	-232.543
	SWCRC	0.964595	172.683	88.4779	71.3949	-288.894
	FNLPR	0.832715	176.551	81.1707	66.9917	-189.771
1AQL	SRGFGF	0.96031	172.16	94.1695	75.723	-192.432
	SWCRC	0.964595	160.666	82.4595	63.3393	-254.913
	FNLPR	0.832715	167.766	77.089	73.6001	-187.692

As shown in Fig. 5(a), the interaction between the three peptides and PL was clearly observed. The ligand SRGFGF formed six hydrogen bonds with the surrounding amino acid residues of PL, including Thr112 (3.04 Å), Ser (2.05 Å), Phe77 (2.17 Å), Gly76 (2.77 Å), His151 (2.65 Å), and His263 (1.83 Å). Hydrogen bond distances are indicated in parentheses. In addition, SRGFGF exhibited hydrophobic interactions with Ile78, Ala260, Leu264, and Ile209. The peptide SWCRC formed a total of thirteen hydrogen bonds with PL, involving residues Phe77 (2.17 Å, 2.57 Å, and 2.79 Å), Gly76 (2.23 Å and 2.91 Å), His151 (2.88 Å), Ser152 (2.14 Å, 2.55 Å, and 3.00 Å), Phe215 (2.65 Å), Ala259 (1.95 Å and 2.48 Å), and His263 (2.35 Å). The ligand FNLPR formed six hydrogen bonds with PL residues Gly76 (2.58 Å), Phe77 (2.07 Å and 4.82 Å), His151 (2.58 Å), and Ser152 (2.67 Å and 2.69 Å). It also engaged in hydrophobic interactions with Phe77, Tyr114, Phe215, Ala178, and Pro180. As shown in Fig. 5(b), the interactions between the peptides and ChE were also characterized. SRGFGF formed five hydrogen bonds with ChE residues Ala108 (2.58 Å), Ala195 (2.51 Å), His435 (2.03 Å), and Ala436 (2.52 Å and 2.57 Å), and exhibited hydrophobic interactions with Phe324, Leu392, and Trp227.SWCRC formed seven hydrogen bonds with ChE residues Gly106 (3.82 Å), Asp (3.09 Å), His (1.89 Å, 2.47 Å, and 2.52 Å), and Asp437 (2.12 Å and 2.25 Å), along with additional hydrophobic interactions with Ala436. FNLPR interacted with ChE through five hydrogen bonds involving Gly107 (2.52 Å), Ala108 (2.18 Å), Glu193 (2.16 Å), Ala195 (2.78 Å), and His (2.83 Å), and also formed hydrophobic contacts with Leu323 and Ala436. Collectively,

these results suggest that all three peptides exhibit strong binding affinities with both PL and ChE, indicating their potential inhibitory activity toward these lipid-metabolizing enzymes.

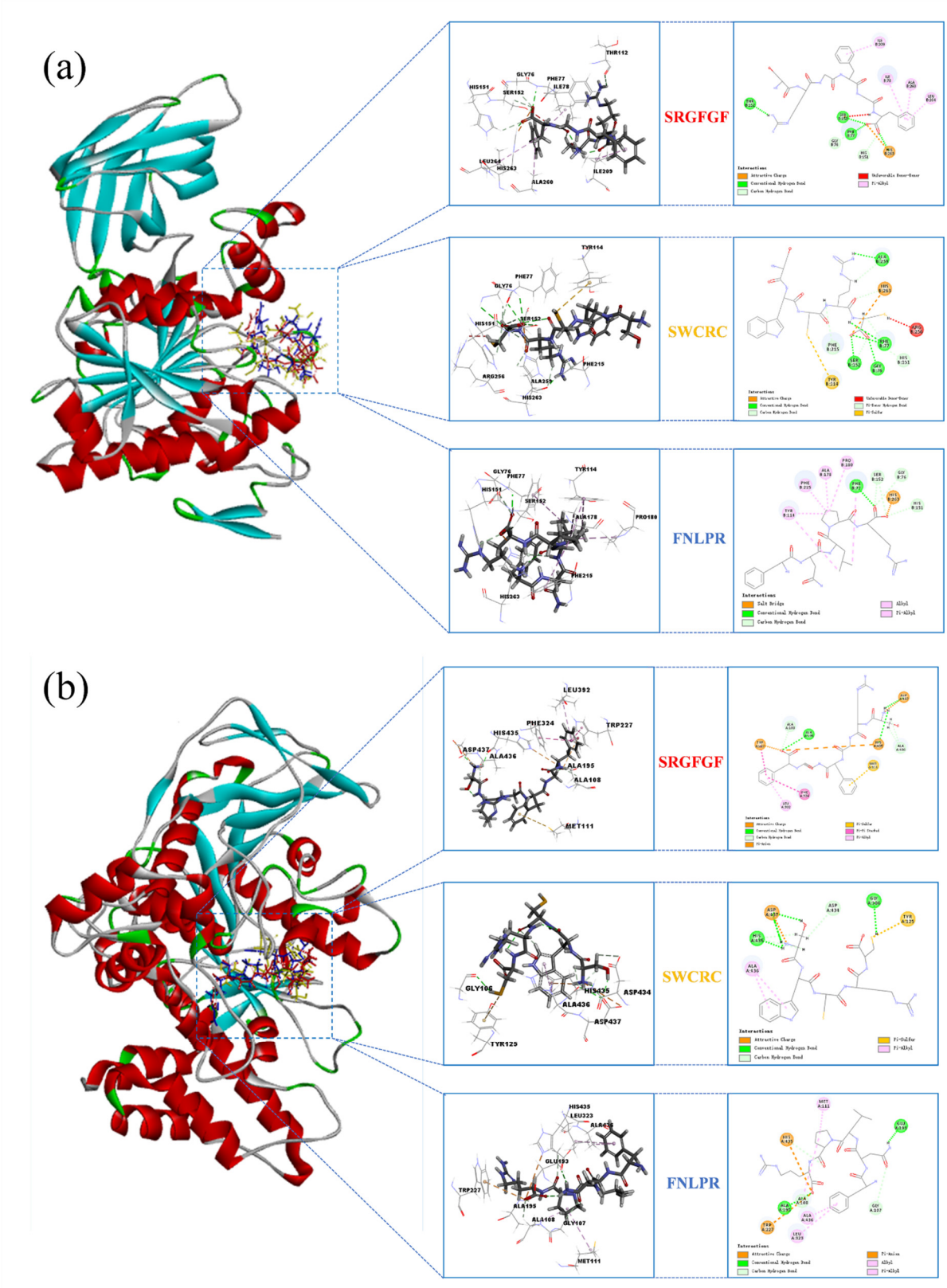

Fig. 5 Docking results of yellow wine lees peptides with PL and ChE molecules. (a) 2D and 3D mechanism diagrams of SRGFGF, SWCRC and FNLPR docked with PL; (b) 2D and 3D mechanism diagrams of SRGFGF, SWCRC and FNLPR docked with ChE.

3.7 In vitro validation results of synthetic peptides for lipid-lowering

To validate the lipid-lowering effects of the three peptides identified through molecular docking (SRGFGF, SWCRC, and FNLPR), these peptides were chemically synthesized and their inhibitory activities against PL and ChE were assessed. As shown in Fig. 6(a-b), all three peptides exhibited inhibitory effects on both enzymes in a dose-dependent manner. Notably, among the tested concentrations (2.0 mmol/L, 1.0 mmol/L, and 0.5 mmol/L), SWCRC consistently demonstrated the strongest inhibitory activity against PL, outperforming SRGFGF and FNLPR. Similarly, SWCRC also showed superior inhibitory activity against ChE at higher concentrations. Due to its potent enzyme inhibition, SWCRC was selected for further investigation. As presented in Fig. 6(c-d), the IC_{50} values of SWCRC against PL and ChE were (1.153 ± 0.14) mmol/L and (6.587 ± 0.228) mmol/L, respectively. Although these values are higher than those of the positive control orlistat IC_{50} = (0.0177 ± 0.0067) mmol/L for PL and IC_{50} = (0.1363 ± 0.0377) mmol/L for ChE, the inhibition gap between SWCRC and orlistat narrowed with increasing concentrations. These results suggest that SWCRC still holds promise as a lipid-lowering agent worthy of further exploration. Compared with traditional pharmaceutical inhibitors, SWCRC, as a peptide, features a modifiable peptide backbone and potentially fewer side effects, indicating its potential as a candidate for the development of novel lipid-lowering therapeutics.

To determine the inhibition type of SWCRC on PL and ChE, the linear regression curves presented in Fig. 6 (e-h) and Table S2 show that the inhibition mode of SWCRC with PL and ChE is consistent with the protein experiments conducted earlier. The regression curves of reaction rates for varying concentrations of SWCRC at different PL and ChE concentrations all intersect the origin and demonstrate reversibility. Reversible inhibition can, in turn, be categorized into competitive, non-competitive, and mixed inhibition based on kinetic characteristics. The inhibitory effect of SWCRC on PL was depicted by a double reciprocal Lineweaver-Burk plot, with the curves intersecting in the second quadrant. This pattern was marked by an elevated K_m value and a reduced V_{max}. This suggests that the inhibition type follows a mixed competitive mode.he inhibitory effect of SWCRC on ChE was characterized by a double reciprocal Lineweaver-Burk plot, where the curves intersected at the positive Y-axis, indicative of a competitive inhibition mechanism.

To further investigate the effects of SWCRC on the microenvironment of amino acid residues in PL and ChE, UV-visible spectroscopy scans were conducted in the range of 200-350 nm for enzyme-peptide complexes at varying concentrations of SWCRC. As shown in Fig. 6(i-j), for PL, two prominent absorption peaks were observed around 216 nm and 260 nm. With increasing concentrations of SWCRC, the intensities of both peaks increased, accompanied by a red shift.In the case of ChE, two major peaks were identified near 208 nm and 220 nm. As the concentration of SWCRC increased, both peaks exhibited subtle red shifts. Additionally, a distinct absorption peak near 269 nm became more pronounced with higher concentrations of SWCRC, also accompanied by a red shift. These observations suggest that SWCRC alters the microenvironment of amino acid residues within PL and ChE, indicating potential changes in enzyme conformation upon peptide binding.

To investigate the effect of SWCRC on the tertiary structure of PL and ChE, fluorescence spectroscopy was performed with excitation at 280 nm and emission scans recorded in the range of 300-500 nm. As shown in Fig. 6(k-l), both the SWCRC-PL and SWCRC-ChE complexes exhibited maximum fluorescence intensity near 330 nm. With increasing concentrations of SWCRC, the fluorescence intensity progressively decreased, indicating that SWCRC exerts a quenching effect on both enzymes. Additionally, a noticeable red shift in the fluorescence emission peaks was observed for both PL and ChE, suggesting conformational changes in the enzyme structures. Table S3 presents K_a, K_q, K_{SV}, and n for SWCRC in complex with PL and ChE. The calculated Kq values were 2.62×10^{10} L/mol·s for PL and 2.90×10^{10} L/mol·s for ChE.

In *in vitro* experiments, SWCRC exhibited the most potent inhibitory effects on PL and ChE among the three screened peptides. Further analysis using reversible competitive inhibition assays, UV-visible spectroscopy, and fluorescence spectroscopy confirmed that SWCRC possesses a notable affinity for both enzymes, maintains stable binding interactions, and induces conformational alterations in their tertiary structures.

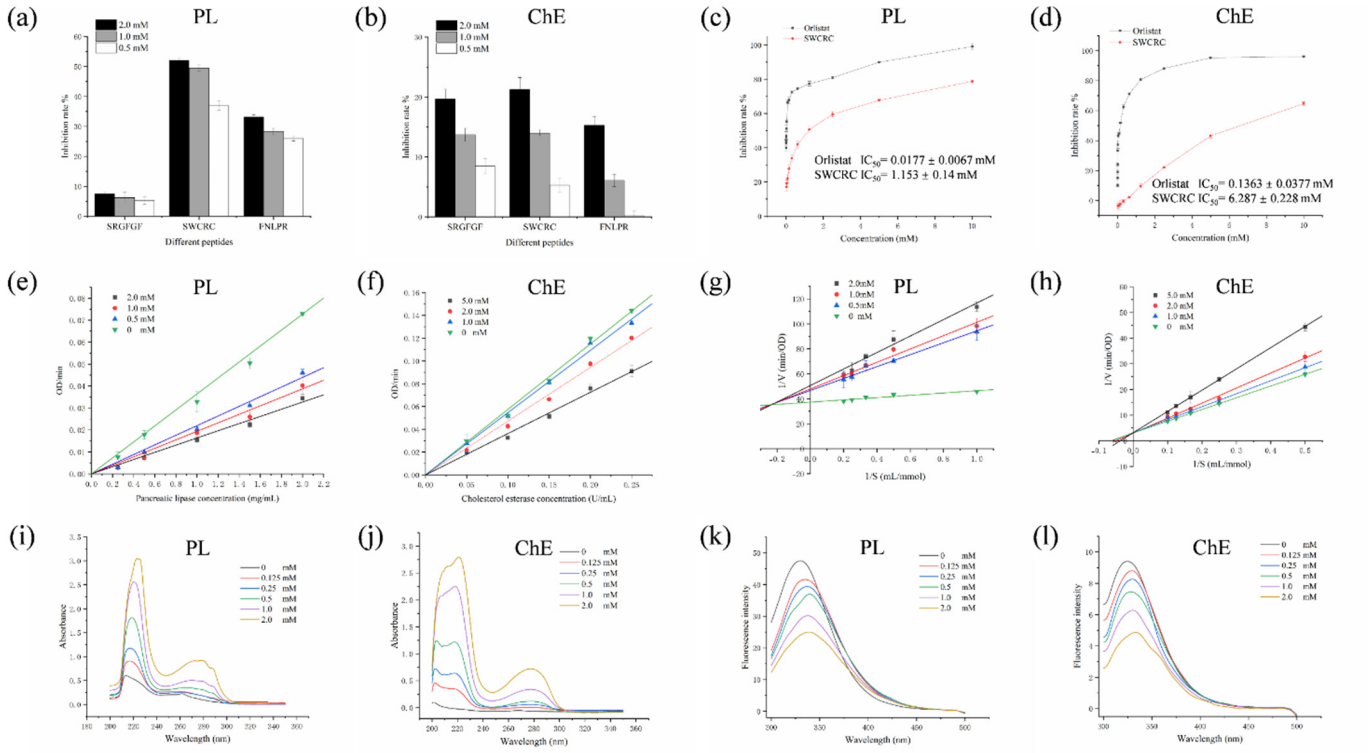

Fig. 6 *In vitro* lipid-lowering activity of synthetic peptides. (a-b) Inhibition of PL and ChE by various synthetic peptides; (c-d) Inhibitory effects of SWCRC on PL and ChE; (e-f) Kinetic curves of SWCRC inhibition of PL and ChE; (g-h) Lineweaver-Burk plots of PL and ChE inhibition by SWCRC; (i-j) UV-visible spectra of PL and ChE with SWCRC; (k-l) Fluorescence spectra of PL and ChE with SWCRC.

3.8 MD simulation analysis results

To further elucidate the inhibitory mechanism of SWCRC on PL and ChE, molecular dynamics (MD) simulations were performed, including analyses of RMSD, Rg, and RMSF for both the enzymes and their peptide-enzyme complexes. The simulation results are shown in Fig. 6. For PL Fig. 6(a-c), the RMSD of the free PL system reached equilibrium at around 8 ns, whereas the PL-SWCRC complex reached equilibrium at approximately 80 ns, with RMSD fluctuations within 0.4 nm, indicating the complex attained structural

stability after SWCRC binding. The average RMSD values for both systems were < 0.45 nm over the 100 ns simulation period. The Rg was used to assess the compactness of the protein structure. Both PL and PL-SWCRC systems exhibited Rg values fluctuating between 2.55 and 2.65 nm, with a fluctuation range of only 0.1 nm. However, the PL-SWCRC complex showed slightly higher Rg values compared to PL alone, suggesting a looser protein structure after SWCRC binding. The RMSF analysis showed that the PL-SWCRC complex exhibited greater fluctuations in residues 240-260, though all RMSF values remained below 2.0 Å. Notably, key residues involved in enzymatic activity (Ser152, His263, and Phe77) had RMSF values below 0.2 Å, indicating that the enzyme-inhibitor complex formed a stable structure and effectively engaged the active site. For ChE Fig. 6(d-f), the RMSD of the ChE-SWCRC complex reached equilibrium rapidly at 8 ns and was significantly lower than that of free ChE, indicating a more stable complex structure. Throughout the 100 ns simulation, both systems maintained average RMSD values < 0.25 nm, with the ChE-SWCRC complex showing tighter binding compared to PL. The Rg values for ChE and ChE-SWCRC fluctuated between 2.33 and 2.37 nm, with minimal variation (Fig. 7). The complex exhibited lower Rg values than free ChE for most of the simulation, suggesting a more compact structure upon SWCRC binding. The average RMSF value for the ChE-SWCRC complex was 0.078 Å, lower than that of PL-SWCRC (0.081 Å), indicating reduced residue mobility. Moreover, the RMSF values for residues Ser194, Asp320, and His435 were below 0.2 Å, supporting the conclusion that SWCRC binding promoted tighter interactions with the active site and enhanced inhibitor stability.

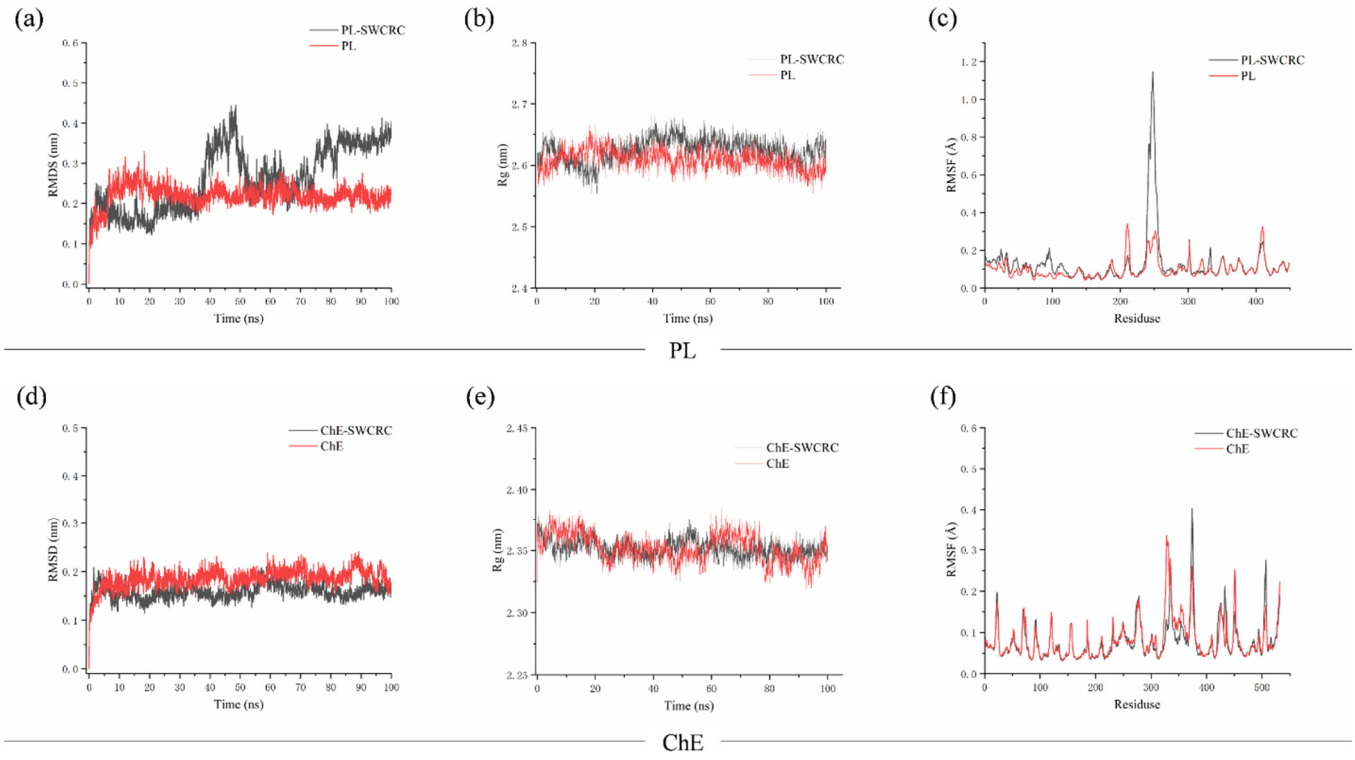

Fig. 7 Molecular dynamics simulations of PL/ChE-SWCRC complexes. (a) RMSD of PL and the PL-SWCRC system; (b) Rg of PL and the PL-SWCRC system;(c) RMSF of PL and the PL-SWCRC system; (d) RMSD of ChE and the ChE-SWCRC system; (e) Rg of ChE and the ChE-SWCRC system; (f) RMSF of ChE and the ChE-SWCRC system.

3.9 Hypolipidemic results of SWCRC on C. elegans model

Previous *in vitro* experiments and molecular simulations both indicated that SWCRC could alter the structures of the two enzymes, thereby exhibiting a notable inhibitory effect. This suggests that SWCRC may possess lipid-lowering potential. However, we believe that further in vivo verification is necessary. Therefore, we employed a *C. elegans* obesity model to evaluate the lipid-lowering effects of the SWCRC peptide in vivo. As shown in Fig. S1, SWCRC at various concentrations (125-2000 μmol/L) did not inhibit the growth of *E. coli* OP50, indicating that this concentration range is suitable for subsequent experiments. The lipid-lowering effects of the peptide in the *C. elegans* model are presented in Fig. 8. From the Oil Red O staining areas in Fig. 8 (a-c), the relative fat content in the model group (88.55 ± 4.22)% was significantly ($P < 0.05$) higher than that of the control group (24.26 ± 4.12)%, confirming the successful establishment of the lipid-accumulation model in *C. elegans*. Fat accumulation decreased progressively with increasing concentrations of SWCRC. Specifically, when SWCRC concentration increased from 125 μmol/L to 2000 μmol/L, the stained area decreased from (76.38 ± 4.02)% to (37.61 ± 2.62)% ($P < 0.05$).

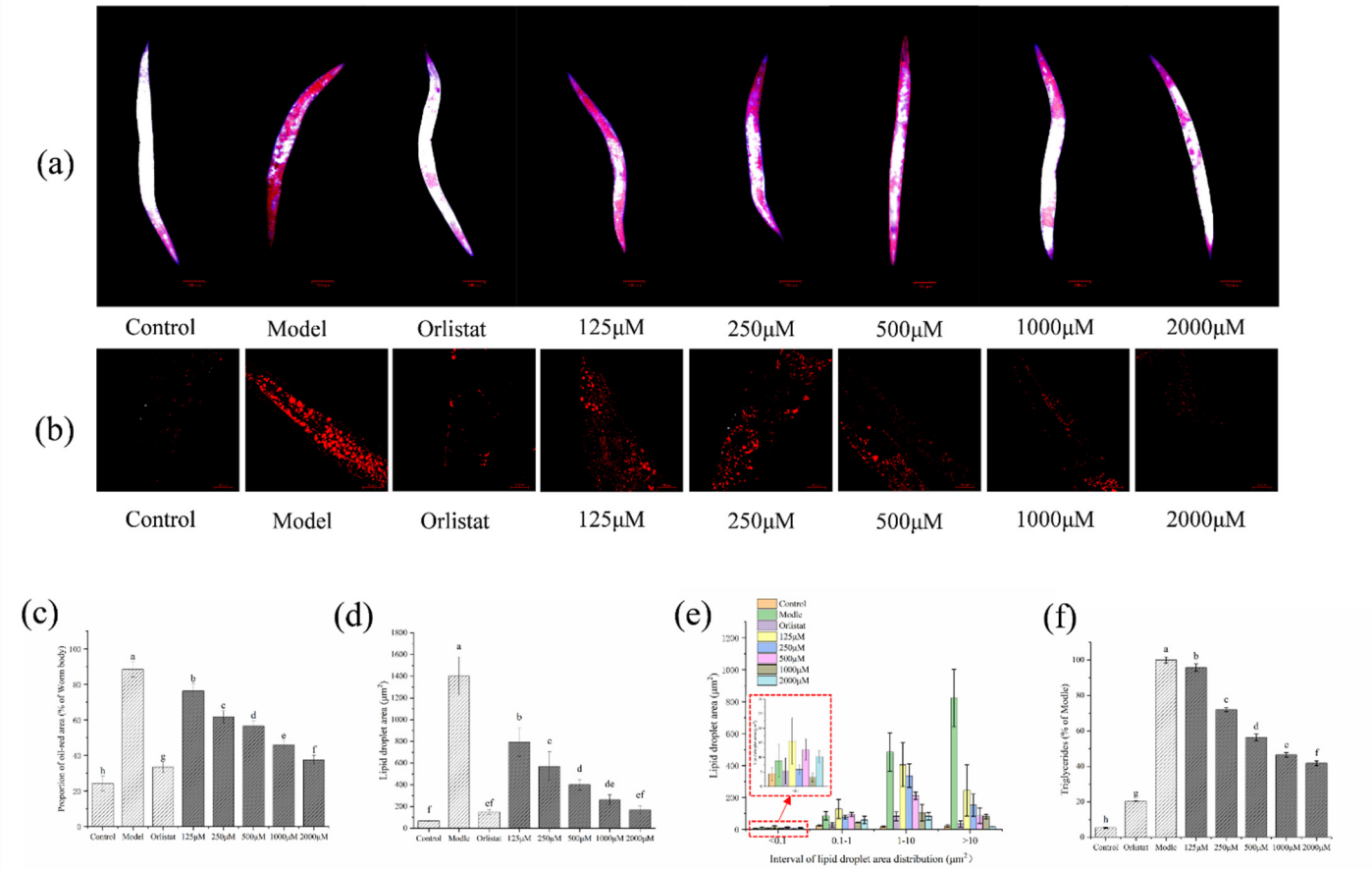

Fig. 8 Lipid-lowering effects of SWCRC in *C. elegans* model. representative photographs of *C. elegans* oil red O (a) and Nile red (b) staining are shown; (c) statistics of the oil red O staining results; (d-e) statistics of the lipid droplet results of the Nile red staining; and (f) results of the TG content test; different letters indicate significant differences between groups ($P < 0.05$).

In addition, Nile Red staining was conducted to further assess the effect of SWCRC on intracellular lipid droplet distribution and fat storage levels in *C. elegans*, as shown in Fig. 8(b, d, e). The total lipid droplet area across different SWCRC concentrations exhibited a trend consistent with the Oil Red O staining results. With increasing concentrations, lipid droplets became more dispersed and their size decreased. Fig. 8(e) shows that the number of droplets sized 1-10 μm² and >10 μm² declined as the SWCRC concentration

increased. Notably, the proportion of lipid droplets smaller than 0.1 μm² relative to the total droplet area was (6.31 ± 2.82)% in the control group, (3.35 ± 2.27)% in the orlistat group, and (6.30 ± 1.56)% in the 2000 μmol/L SWCRC group. The 2000 μmol/L group showed a distribution pattern similar to the control and superior to orlistat, suggesting that SWCRC effectively promoted lipid droplet dispersion.

To further explore the lipid-lowering effect of SWCRC, we measured the TG content in *C. elegans* treated with various SWCRC concentrations, as shown in Fig. 8(f). Compared to the model group, SWCRC treatment (125-2000 μmol/L) resulted in a significant reduction in TG levels ($P < 0.05$), with a maximum decrease of (41.79 ± 1.32)%. Although the reduction was not as substantial as that achieved by orlistat, the effect can still be considered ideal for a non-pharmaceutical peptide.

In summary, the *C. elegans* model effectively demonstrated the in vivo lipid-lowering capacity of SWCRC, consistent with previous in vitro findings. These results confirm that SWCRC is a lipid-lowering bioactive peptide that can be isolated fromYWLP.

4. Discussion

Cereal protein peptides have a wide range of biological activities [35]. Given the high protein content in the dry yellow wine lees used in this study, this material holds significant potential for development. Its protein components can be further explored and utilized for the discovery and identification of bioactive peptides.

SDS-PAGE analysis of YWLP revealed that the proteins obtained through simple alkali extraction and acid precipitation were already of relatively low molecular weight. Compared to the results reported by Chin et al. (Chin et al., 2022) for extracted lees proteins, the proteins extracted in this study exhibited smaller molecular weights. This difference may be attributed to the higher protease activity or longer fermentation time involved in yellow wine lees production, which could result in more extensive hydrolysis of proteins into smaller peptide fragments. Therefore, the enzymatic hydrolysis step may be omitted in this study, allowing direct screening of lipid-lowering peptides from lees protein, thereby improving the utilization and economic value of yellow wine lees.

There is a close relationship between antioxidant and hypolipidemic activities [36]. Antioxidants can reduce oxidative stress, thereby protecting lipids from oxidative damage and helping to maintain stable blood lipid levels [37]. YWLP exhibited strong scavenging activity against ABTS, DPPH, and O_2^- radicals. Furthermore, low-molecular-weight proteins are known to exhibit higher antioxidant activity [7], and the molecular weight of YWLP is predominantly below 25 kDa, which aligns with this finding. Therefore, YWLP shows promising potential for the development of hypolipidemic agents.

According to previous studies, PL and ChE are two key enzymes involved in lipid-lowering activity and mechanisms [8]. PL plays a critical role in the hydrolysis of dietary fats, and inhibiting its activity can effectively reduce fat absorption efficiency in the small intestine, thereby achieving a lipid-lowering effect [24, 38]. Inhibiting ChE activity can slow down the conversion of cholesterol esters into free cholesterol, thereby reducing the rate at which cholesterol is absorbed by the human body and lowering plasma

cholesterol levels [39]. The results showed that the IC_{50} of YWLP against PL was (0.351 ± 0.0922) mg/mL, which is approximately 175 times higher than that of the positive control orlistat IC_{50} = (0.0020 ± 0.0005) mg/mL for pancreatic lipase. For ChE, YWLP exhibited an IC_{50} of (0.2621 ± 0.0192) mg/mL, which is only 3.44 times higher than that of orlistat IC_{50} = (0.0763 ± 0.0059) mg/mL. Orlistat is a purified pharmaceutical agent with strong and specific inhibitory activity against PL [40]. In contrast, YWLP is a crude bioactive extract derived from wine lees, yet it has already demonstrated significant inhibitory effects on both enzymes. Based on its interaction with enzyme activity, inhibitors can be categorized into two types: reversible and irreversible inhibitors [41]. Irreversible inhibitors covalently bind to enzymes, resulting in permanent deactivation. While this can enhance efficacy, it may also lead to adverse reactions and specificity-related toxicity. In contrast, reversible inhibitors form temporary complexes with enzymes through non-covalent interactions, thereby avoiding these risks and potentially improving drug delivery efficiency. The results showed that the plots for both PL and ChE inhibition by YWLP passed through the origin when the YWLP concentration was varied, indicating that YWLP can be considered a safe and reversible inhibitor of PL and ChE.

Bile acids are the main components of bile and are derived from the metabolism and breakdown of cholesterol in the liver, making them a major end product of cholesterol metabolism in humans. In the human body, bile acids primarily exist in the form of bile salts [21]. Studies have found that YWLP exhibits a certain level of binding affinity to bile salts. Notably, Compared to SC binding effect, YWLP showed a stronger binding affinity to STC, which may be consistent with the findings of Yang et al. [42]. The molecular structure of STC contains a taurine group, which may interact more readily with specific components in the sample, thereby enhancing binding energy. Cholesterol micelles play a vital role in intestinal cholesterol absorption. Interfering with the assembly of these micelles can effectively reduce cholesterol uptake in the intestine [42]. YWLP was found to significantly inhibit the solubility of cholesterol micelles. These findings provide a solid basis for the potential application of yellow wine lees in screening lipid-lowering peptides and in the development of novel functional foods or therapeutic agents for lipid regulation.

Cell viability above 90% is generally not considered cytotoxic [43]. Therefore, the main focus of the subsequent experiments was to consider cellular experiments with 0-500 μg/mL YWLP concentrations. Elevated lipid levels are a key contributing factor to hyperlipidemia [18]. Through Oil Red O staining, it was observed that YWLP exhibited lipid-regulating effects even at lower concentrations. Compared with the model group, the proportion of red-stained lipid droplets was significantly reduced ($P < 0.05$), indicating that YWLP can decrease lipid accumulation and regulate lipid metabolism in high-fat cell models. Liver dysfunction, as reflected by abnormal levels of AST and ALT, may suggest disrupted hepatic lipid metabolism, which in turn can affect systemic lipid levels. Key indicators of lipid profile, including TC, TG, and HDL-C, are critical parameters linked to cardiovascular health. Elevated TC and TG are associated with increased cardiovascular risk, whereas higher HDL-C is considered protective [44]. In this study, YWLP was

found to exert beneficial effects on all five lipid-related indicators, thereby effectively alleviating hyperlipidemia [45].

To obtain peptides with stronger antihyperlipidemic activity, separation and purification are essential [46]. Ultrafiltration is a commonly used technique for separating or concentrating target components [47], and it was applied to verify the lipid-lowering activity of YWLP with different molecular weights. The results showed that the < 3 kDa fraction exhibited the most significant activity. This outcome could be attributed to the spatial hindrance encountered by higher molecular weight peptides when interacting with the active sites of PL and ChE. In contrast, shorter peptides, with fewer amino acids and lower molecular weights, exhibit superior inhibitory activity. This finding is consistent with previous research on peptide binding [8, 48]. Therefore, to further identify lipid-lowering peptides, LC-MS/MS analysis was conducted on the < 3 kDa YWLP fraction. The enhanced bioactivity observed in this fraction is likely due to the predominance of < 1 kDa peptides, as demonstrated by Wang et al. [49, 50], who showed that short peptides have stronger inhibitory effects on PL and ChE. It is noteworthy that among the five most abundant amino acids in this fraction, the majority are hydrophobic, a composition known to be favorable for lipid-lowering activity [46]. Moreover, the lipid-lowering activity of peptides is closely associated with their pI; peptides with acidic pI values are more likely to exhibit enhanced antihyperlipidemic activity. [51]. Finally, a proper hydrophilic-hydrophobic balance contributes to both the biological activity and structural stability of peptides [52].

Computational molecular docking is capable of forecasting the interaction and orientation of ligands with macromolecular receptors. This method can elucidate the mechanism of receptor-ligand interactions by directly examining the binding configurations and sites of both the receptor and ligand [53]. Virtual screening is an effective strategy for identifying novel lead compounds [54] and has been widely employed in the prediction of antihyperlipidemic peptide activity [46]. For instance, Ye et al. [8] used molecular docking to identify peptides with favorable binding energies to PL and ChE, predicting their potential lipid-lowering effects, which were subsequently validated through in vitro experiments. In this study, results obtained from DS2019 identified SRGFGF, SWCRC, and FNLPR as the top three candidate peptides. Visualization revealed that these peptides mainly interacted with the PL and ChE receptors through hydrogen bonding and hydrophobic interactions. These two types of interactions are fundamental for stabilizing ligand-receptor complexes [55, 56], playing a crucial role in maintaining the spatial structure of the complexes. Thus, these peptides are inferred to have the potential to inhibit the enzymatic activities of PL and ChE. In the PL docking analysis, SRGFGF formed a hydrogen bond with the His263 residue of PL, with a bond length of only 1.83 Å, which may explain its highest -CDOCKER ENERGY score. In contrast, SWCRC formed the greatest number of hydrogen bonds with PL residues, possibly contributing to its lowest binding energy. Notably, four key (GLY76, PHE77, HIS151, and SER152) residues in PL were found to form hydrogen bonds with all three peptides. Among them, Phe77 acts as both a hydrogen bond donor and an electrostatic stabilizer, contributing to the formation of the oxyanion hole necessary for substrate hydrolysis. The

interaction of all three peptides with Phe77 suggests a potential mechanism underlying their inhibitory effects on pancreatic lipase. In ChE, all three peptides were observed to form hydrogen bonds with the key active site residue His435. The primary catalytic triad of ChE includes Ser194, His435, and Asp320 [9], indicating that these peptides likely exhibit strong inhibitory activity against ChE. Furthermore, SRGFGF had the highest -CDOCKER ENERGY score, while SWCRC showed the lowest binding energy in docking with ChE, consistent with the PL docking results. Specifically, SRGFGF formed a hydrogen bond with Asp437 at a bond length of just 1.76 Å, and SWCRC exhibited the greatest number of hydrogen bonds among the three peptides. In addition, on closer inspection we can find that among these three peptides (SRGFGF, SWCRC and FNLPR), all of them share similar features in the peptide chain, having arginine (R), which is the amino acid found more frequently in the LC-MS/MS identification of wine lees peptides. This characterization with arginine is consistent with the results of the PL inhibitory peptide screened from *Seabuckthorn* seed meal by Xiang et al. [57]. Therefore, these three peptides derived from YWLP are structurally validated to possess inhibitory activity against lipid-lowering enzymes.

Numerous studies have demonstrated that peptides are effective inhibitors of PL and ChE. Zhang et al. [58] conducted virtual screening followed by in vitro validation and identified five tripeptides (IWR, FWY, VFR, VWW, and FYF) with PL inhibitory IC_{50} values ranging from 0.230 to 1.165 mg/mL, and ChE IC_{50} values ranging from 0.214 to 0.667 mg/mL. Similarly, Huang et al. [19] reported that four peptides (AINDPFIDL, FLGM, GLLF, and WGPL) isolated from *Katsuwonus pelamis* exhibited significant inhibitory effects on PL and ChE, with GLLF showing IC_{50} values of 0.1891 mg/mL (PL) and 0.2534 mg/mL (ChE), and further mechanistic investigations were conducted. In another study, Zhang et al. [59] identified a lipid-lowering peptide VPPP from *Protaetia brevitarsis*, which showed PL and ChE inhibitory IC_{50} values of (1.81 ± 0.22) mg/mL and (1.62 ± 0.31) mg/mL, respectively. When compared to these previous findings, the peptide SWCRC identified in the present study exhibited relatively modest inhibitory activity, with IC_{50} values of (1.153 ± 0.14) mmol/L (PL) and (6.587 ± 0.228) mmol/L (ChE). Despite not showing superior inhibition in terms of IC_{50} values, SWCRC remains of significant interest due to its unique sequence and potential for multi-target modulation of lipid metabolism, which may contribute to improved lipid-lowering effects in vivo. Moreover, this study highlights the value of reusing byproducts such as yellow wine lees, promoting sustainable development within the brewing industry.

The inhibition pattern of SWCRC against PL follows a mixed competitive model, indicating that SWCRC can bind not only to the active site of PL but also to other allosteric sites. This dual binding capacity provides greater flexibility in modulating enzymatic activity, which enhances its potential in drug development and biochemical research [60]. In addition, SWCRC exhibits competitive inhibition against ChE, where it binds directly to the enzyme's active site, effectively blocking substrate access. Many therapeutic agents have been shown to regulate enzyme activity through competitive inhibition mechanisms, making this mode of action a well-established strategy in disease treatment [61].

UV-visible absorption spectroscopy is a valuable method for assessing conformational changes in enzyme proteins. Variations in the UV-visible absorbance of chromophores within amino acid residues can provide insights into alterations in protein structure and stability (Huang et al., 2020). In this study, the UV-visible absorption spectra of PL in the presence of varying concentrations of SWCRC were consistent with the findings of Chen et al. (Chen et al., 2021). As the concentration of SWCRC increased, the absorption peak intensity also increased, accompanied by a red shift. This red shift indicates an increase in the hydrophobicity of the enzyme's microenvironment, suggesting alterations in its secondary structure [62]. A strong absorption peak near 216 nm reflects the backbone structure of the enzyme, while the peak at 260 nm corresponds to aromatic amino acid residues (Trp, Tyr, or Phe), associated with $\pi \rightarrow \pi^*$ transitions [63]. These spectral changes were further supported by molecular docking results, which revealed that SWCRC forms hydrogen bonds with Phe77 and Phe152 in PL, and engages in Pi-Sulfur interactions with Tyr114. For ChE, an additional absorption peak was observed at 204 nm, likely associated with ester bond-related chromophores. Absorption peaks at 220 nm and 269 nm mirrored those found in PL. Molecular docking also revealed a Pi-Sulfur interaction between SWCRC and Tyr125 in ChE. These findings collectively underscore the significant interactions between SWCRC and both PL and ChE, which likely induce local unfolding or relaxation within the enzyme frameworks, consequently affecting their structural integrity and stability [58].

Fluorescence spectroscopy is highly sensitive to the polarity of the surrounding environment, as intrinsic fluorescence is exhibited by aromatic amino acids (Trp, Tyr, Phe) [64]. Both PL and ChE contain these aromatic groups, producing a single fluorescence emission peak near 330 nm. A decrease in fluorescence intensity typically indicates an increase in the polarity of the surrounding environment or the exposure of aromatic residues, which reflects structural perturbations within the enzyme [65]. Upon the addition of SWCRC, changes in the microenvironment of the amino acid residues within the enzyme systems were observed, accompanied by a red shift in the emission peak. This red shift signifies a disturbance in the rigidity of the protein structure, resulting in conformational relaxation [66] that may facilitate deeper insertion of SWCRC into the protein matrix. Consequently, the affinity of aromatic residues for SWCRC increases, which is consistent with the results obtained from molecular docking and UV-visible spectroscopy. Furthermore, the fluorescence quenching mechanism of SWCRC toward both enzymes was identified as static quenching, as evidenced by a quenching rate constant exceeding the average diffusion-controlled dynamic quenching rate (2.00×10^{10} mol/L·s)[32].

MD simulation is a powerful computational technique that enables detailed investigation of enzyme conformational changes, active site dynamics, and protein-substrate interactions, thereby offering theoretical insights into enzymatic catalytic mechanisms [67] [68]. Among them, the RMSD value is an important indicator for assessing the change in stability of complex conformations, Rg is an important parameter for studying the structural densities of proteins during simulation, and the RMSF value refers to the structural deviation from the initial protein structure [69].In most enzyme activity studies involving molecular dynamics

simulations, RMSD, Rg and RMSF are the three primary parameters analyzed. In the present study, the RMSD of the PL-SWCRC complex exhibited greater fluctuations compared to the enzyme-only system, whereas the ChE-SWCRC complex showed the opposite trend. A higher RMSD typically indicates reduced structural stability of the protein system [68]. Therefore, overall, the ChE-SWCRC complex demonstrated better binding stability. The Rg value reflects the degree of compactness of the complex; larger Rg values indicate a more expanded structure and increased system relaxation [70], while smaller Rg values suggest a more compact and stable conformation [71]. Both the PL-SWCRC and ChE-SWCRC complexes showed relatively small Rg values throughout the MD simulation, suggesting that the enzyme-inhibitor complexes maintained stable structures[72]. Notably, at the early stage of the simulation, the Rg values of the enzyme-inhibitor complexes were higher than those of the free enzyme systems, indicating that SWCRC initially induced a conformational relaxation of the enzyme, potentially leading to disruption of catalytic site integrity. Additionally, the RMSF values of the complexes were relatively low, further confirming the stability of the systems [73]. The ChE-SWCRC complex exhibited lower RMSF values, indicating that the enzyme maintained a relatively rigid conformation upon inhibitor binding, with minimal structural fluctuations.Notably, the PL-SWCRC complex exhibited higher RMSF values at certain amino acid residues, indicating regions of increased flexibility [74]. This local flexibility may allow for a greater diversity of binding interactions between SWCRC and PL compared to ChE, which could partly explain the lower IC_{50} value of SWCRC against PL.

C. elegans serves as an ideal model organism for studying lipid metabolism and obesity-related genetics due to its highly conserved mechanisms of fat storage and metabolic regulation shared with mammals [75]. Lipid droplets in *C. elegans* are predominantly stored in subcutaneous cells and around the intestinal region [76], and their distribution can be visualized using Oil Red O and Nile Red staining techniques [76]. In this study, Oil Red O staining revealed that SWCRC significantly reduced lipid accumulation in *C. elegans*. Consistently, Nile Red staining further demonstrated that SWCRC markedly decreased and dispersed lipid content in the worms. Lipid droplet size and distribution are closely associated with metabolic regulation [77]. Studies have shown that smaller lipid droplets possess a relatively larger surface area, which significantly enhances the accessibility of lipolytic enzymes, thereby promoting lipid breakdown [75]. This suggests that SWCRC may reduce lipid accumulation in *C. elegans* by limiting both the number and size of lipid droplets. In animals, fat is primarily stored in the form of TG, which serve as a key endpoint indicator for evaluating lipid metabolism interventions [34, 75]. However, Oil Red O staining cannot distinguish TG from other lipid-soluble compounds [78]. Further validation in this study revealed that SWCRC also significantly suppressed TG accumulation in *C. elegans*, confirming its lipid-lowering potential at the metabolic level.

5. Conclusion

This study employed multiple methods to confirm the hypolipidemic activity of YWLP and subsequently screened hypolipidemic peptides from wine lees using LC-MS/MS and computational analysis.

Proteins with hypolipidemic effects were initially prepared using alkaline extraction and acid precipitation, followed by the verification of YWLP's hypolipidemic activity through antioxidant assays, enzyme (PL and ChE) activity tests, bile acid salt binding assays, cholesterol micelle assays, and cellular experiments. Notably, YWLP exhibited strong inhibition of ChE and PL, with ChE inhibition by crude proteins from the lees being comparable to that of orlistat. Three lipid-lowering peptides (SRGFGF, SWCRC, and FNLPR) were identified from 3880 peptides through protein ultrafiltration, characterization, and molecular docking screening. Based on the docking results, all three peptides demonstrated strong binding to PL and ChE. The three peptides were then synthesized, and *in vitro* experiments confirmed that SWCRC exhibited optimal PL and ChE inhibitory activities. Enzyme kinetics, fluorescence spectroscopy, MD simulations, and UV-visible spectroscopy revealed the inhibition mechanism of SWCRC, which demonstrated strong binding to the active PL sites Ser152, His263, and Phe77, as well as to the ChE sites Ser194, Asp320, and His435. Additionally, the C. *elegans* model was used to evaluate the lipid-lowering effects of SWCRC through Oil Red O staining, Nile Red staining, and TG content measurement. The results consistently demonstrated a significant ($P < 0.05$) lipid-lowering effect of SWCRC *in vivo*. This study introduces an innovative perspective on the development and application of wine lees while providing a foundational framework for advancing research on bioactive hypolipidemic peptides, thereby bridging resource valuation with nutraceutical discovery.

Author contributions

Hongpeng Yu: Conceptualization, Supervision, Writing -review & editing. **Cansheng Ou**: Conceptualization, Writing - original draft, Data curation, Methodology, Investigation. **Dong He**: Conceptualization, Writing - review & editing, Methodology, Supervision, Funding acquisition. **JinJin Yang**: Methodology, Writing - review & editing. **Kegang Wu**: Conceptualization, Writing - review & editing, Supervision. **ZhengXiang Cui**: Methodology, Writing - review & editing. **Xianghua Chai**: Writing - review & editing, Methodology. **Yongqi Cheng:** Methodology, Writing - review & editing. **Wenhui Li:** Writing - review & editing, Methodology. **Xuejuan Duan**: Writing - review & editing, Methodology. **Chenghua Wang:** Methodology, Software. **Shengli Wang**: Writing - review & editing, Methodology.

Acknowledgments

This work was supported by the Science and technology plan project of Heyuan City (220705101471437), the Science & Technology Planning Project of Guangzhou City (2024E04J0379, 202103000078, 202206010181), the Guangxi Science and Technology Programunder Grant (No.AB25069487).

Conflict of interest

The authors have no relevant financial or non-financial interests to disclose.

References

[1] H. Yu, Y. Xiang, K. Wu, et al., Green synthesis of carbon dots from Hakka yellow wine lees: Characterization and applications for Fe3+ and NaFeEDTA sensing, LWT. 208 (2024) 116744. https://doi.org/https://doi.org/10.1016/j.lwt.2024.116744.

[2] M. Qian, F. Ruan, W. Zhao, et al., The dynamics of physicochemical properties, microbial community, and flavor metabolites during the fermentation of semi-dry Hakka rice wine and traditional sweet rice wine, Food Chemistry. 416 (2023) 135844. https://doi.org/https://doi.org/10.1016/j.foodchem.2023.135844.

[3] M. Qian, F. Ruan, W. Zhao, et al. Comparison Study of the Physicochemical Properties, Amino Acids, and Volatile Metabolites of Guangdong Hakka Huangjiu. *Foods.* 12. 2023.

[4] W. Zhao, M. Qian, H. Dong, et al., Effect of Hong Qu on the flavor and quality of Hakka yellow rice wine (Huangjiu) produced in Southern China, LWT. 160 (2022) 113264. https://doi.org/https://doi.org/10.1016/j.lwt.2022.113264.

[5] S. Yang, H. Wang, W. Bai, et al., Valorization of Hakka Huangjiu lees: Optimization of ultrasound-assisted enzymatic extraction and identification of angiotensin I-converting enzyme inhibitory peptides, Food and Bioproducts Processing. 146 (2024) 77-88. https://doi.org/https://doi.org/10.1016/j.fbp.2024.05.010.

[6] L.N. Kong, S.T. Ge, Y. Yang, et al., Pyrolysis mechanism and pyrolysis kinetics of yellow wine lees, Rsc Advances. 14 (2024) 16951-16959. https://doi.org/10.1039/d4ra01541j.

[7] S. Hu, S. Zhu, J. Luo, et al., Effect of extrusion on physicochemical properties and antioxidant potential of protein isolate derived from Baijiu vinasse, Food Chemistry. 384 (2022) 132527. https://doi.org/https://doi.org/10.1016/j.foodchem.2022.132527.

[8] H. Ye, Y. Xu, Y. Sun, et al., Purification, identification and hypolipidemic activities of three novel hypolipidemic peptides from tea protein, Food Research International. 165 (2023) 112450. https://doi.org/https://doi.org/10.1016/j.foodres.2022.112450.

[9] F. Fisayo Ajayi, P. Mudgil, C.-Y. Gan, et al., Identification and characterization of cholesterol esterase and lipase inhibitory peptides from amaranth protein hydrolysates, Food Chemistry: X. 12 (2021) 100165. https://doi.org/https://doi.org/10.1016/j.fochx.2021.100165.

[10] M.R. Ferreira, A.G. Garzón, M.E. Oliva, et al., Lipid-lowering effect of microencapsulated peptides from brewer's spent grain in high-sucrose diet-fed rats, Food Bioscience. 49 (2022) 101981. https://doi.org/https://doi.org/10.1016/j.fbio.2022.101981.

[11] N.A. Lunagariya, N.K. Patel, S.C. Jagtap, et al., Inhibitors of pancreatic lipase: State of the art and clinical perspectives, EXCLI Journal. 13 (2014) 897-921. https://www.scopus.com/inward/record.uri?eid=2-s2.0-84907660761&partnerID=40&md5=6d278cb43ceec4fa60b7dbf5e5933236

[12] X. Zhao, R. Gao, C. Cui, et al., Structural characteristics, functional properties and in vitro

digestibility of rice protein prepared from rice wine lees via an alkaline extraction process or carbohydrate-lipid removal process, Journal of Cereal Science. 117 (2024) 103913. https://doi.org/https://doi.org/10.1016/j.jcs.2024.103913.

[13] Y. Wu, X. Zhang, H. Cui, et al., Isolation, identification and activity analysis of antioxidant peptides from rice wine lees, Journal of Food Measurement and Characterization. 18 (2024) 1528-1542. https://doi.org/10.1007/s11694-023-02244-5.

[14] R. Zhang, Z. Zhou, Z. Ji, et al., Identification and characterization of novel dual-function antioxidant and umami peptides from protein hydrolysates of Huangjiu lees, Food Quality and Safety. 8 (2024) fyae011. https://doi.org/10.1093/fqsafe/fyae011.

[15] Y.M. Wang, X. Pan, Y. He, et al., Hypolipidemic Activities of Two Pentapeptides (VIAPW and IRWWW) from Miiuy Croaker *Miichthys miiuy* Muscle on Lipid Accumulation in HepG2 Cells through Regulation of AMPK Pathway, Applied Sciences-Basel. 10 (2020) 817. https://doi.org/10.3390/app10030817.

[16] J.J. Zhou, M.F. Chen, S.J. Wu, et al., A review on mushroom-derived bioactive peptides: Preparation and biological activities, Food Research International. 134 (2020) 109230. https://doi.org/10.1016/j.foodres.2020.109230.

[17] Q.Y. Zhao, Y.M. Fan, L.X. Zhao, et al., Identification and molecular binding mechanism of novel pancreatic lipase and cholesterol esterase inhibitory peptides from heat-treated adzuki bean protein hydrolysates, Food Chemistry. 439 (2024) 138129. https://doi.org/10.1016/j.foodchem.2023.138129.

[18] H.D. Ye, Y. Xu, Y.N. Sun, et al., Purification, identification and hypolipidemic activities of three novel hypolipidemic peptides from tea protein, Food Research International. 165 (2023) 112450. https://doi.org/10.1016/j.foodres.2022.112450.

[19] F. Huang, Q. Dai, K. Zheng, et al., Exploring the inhibitory potential of KPHs-AL-derived GLLF peptide on pancreatic lipase and cholesterol esterase activities, Food Chemistry. 439 (2024) 138108. https://doi.org/https://doi.org/10.1016/j.foodchem.2023.138108.

[20] F. Yang, J. Huang, H. He, et al., Study on the hypolipidemic activity of rapeseed protein-derived peptides, Food Chemistry. 423 (2023) 136315. https://doi.org/https://doi.org/10.1016/j.foodchem.2023.136315.

[21] Z.-Q. Zhang, X.-R. Ren, J. Geng, et al., Identification, characterization and hypolipidemic effect of novel peptides in protein hydrolysate from Protaetia brevitarsis larvae, Food Research International. 176 (2024) 113813. https://doi.org/https://doi.org/10.1016/j.foodres.2023.113813.

[22] Q. Zhang, Z. Yu, W. Zhao, Identification and action mechanism of novel antioxidative peptides from copra meal protein, LWT. 188 (2023) 115425. https://doi.org/https://doi.org/10.1016/j.lwt.2023.115425.

[23] Y.-M. Wang, X.-Y. Li, J. Wang, et al., Antioxidant peptides from protein hydrolysate of skipjack tuna milt: Purification, identification, and cytoprotection on H2O2 damaged human umbilical vein

endothelial cells, Process Biochemistry. 113 (2022) 258-269. https://doi.org/https://doi.org/10.1016/j.procbio.2022.01.008.

[24] A. Kumar, S. Chauhan, Pancreatic lipase inhibitors: The road voyaged and successes, Life Sciences. 271 (2021) 119115. https://doi.org/https://doi.org/10.1016/j.lfs.2021.119115.

[25] Y. He, X. Pan, C.-F. Chi, et al., Ten new pentapeptides from protein hydrolysate of miiuy croaker (Miichthys miiuy) muscle: Preparation, identification, and antioxidant activity evaluation, LWT. 105 (2019) 1-8. https://doi.org/https://doi.org/10.1016/j.lwt.2019.01.054.

[26] N. Zhang, Y. Zhao, Y. Shi, et al., Polypeptides extracted from Eupolyphaga sinensis walker via enzymic digestion alleviate UV radiation-induced skin photoaging, Biomedicine & Pharmacotherapy. 112 (2019) 108636. https://doi.org/https://doi.org/10.1016/j.biopha.2019.108636.

[27] C.Q. Lu, Q.Y. Gu, X.B. Yu, Effect of *in vitro* simulated digestion on the physicochemical properties and pancreatic lipase inhibitory activity of fucoidan, JOURNAL OF THE SCIENCE OF FOOD AND AGRICULTURE. 104 (2024) 4157-4164. https://doi.org/10.1002/jsfa.13297.

[28] F.F. Huang, Q.F. Dai, K.W. Zheng, et al., Exploring the inhibitory potential of KPHs-AL-derived GLLF peptide on pancreatic lipase and cholesterol esterase activities, FOOD CHEMISTRY. 439 (2024) 138108. https://doi.org/10.1016/j.foodchem.2023.138108.

[29] Y. Hu, D. Wang, Y. Zhang, et al., A novel polysaccharide from blueberry leaves: Extraction, structural characterization, hypolipidemic and hypoglycaemic potentials, Food Chemistry. 460 (2024) 140493. https://doi.org/https://doi.org/10.1016/j.foodchem.2024.140493.

[30] Y. Sun, K. Yang, X. Zhang, et al., In vitro binding capacities, physicochemical properties and structural characteristics of polysaccharides fractionated from Passiflora edulis peel, Food Bioscience. 50 (2022) 102016. https://doi.org/https://doi.org/10.1016/j.fbio.2022.102016.

[31] H. Shen, J. Wang, J. Ao, et al., The inhibitory mechanism of pentacyclic triterpenoid acids on pancreatic lipase and cholesterol esterase, Food Bioscience. 51 (2023) 102341. https://doi.org/https://doi.org/10.1016/j.fbio.2022.102341.

[32] R. Huang, Y. Zhang, S. Shen, et al., Antioxidant and pancreatic lipase inhibitory effects of flavonoids from different citrus peel extracts: An in vitro study, Food Chemistry. 326 (2020) 126785. https://doi.org/https://doi.org/10.1016/j.foodchem.2020.126785.

[33] C.X. Lin, Y.Z. Lin, T.M. Meng, et al., Anti-fat effect and mechanism of polysaccharide-enriched extract from *Cyclocarya paliurus* (Batal.) Iljinskaja in *Caenorhabditis elegans*, Food & Function. 11 (2020) 5320-5332. https://doi.org/10.1039/c9fo03058a.

[34] J. Bai, J. Li, R.R. Pan, et al., Polysaccharides from *Volvariella volvacea* inhibit fat accumulation in *C. elegans* dependent on the aak-2/nhr-49-mediated pathway, Journal of Food Biochemistry. 45 (2021) e13912. https://doi.org/10.1111/jfbc.13912.

[35] X. Gong, A. Qi, L. Liqing, et al., Prospects of cereal protein-derived bioactive peptides: Sources, bioactivities diversity, and production, Critical Reviews in Food Science and Nutrition. 62 (2022) 2855-2871.

https://doi.org/10.1080/10408398.2020.1860897.

[36] Y. Wu, H. Jiang, J.-S. Lin, et al., Antioxidant, Hypolipidemic and Hepatic Protective Activities of Polysaccharides from Phascolosoma esculenta, Marine Drugs. 18 (2020) 158. https://www.mdpi.com/1660-3397/18/3/158

[37] Z. Yang, S. Song, L. Li, et al., Association between the composite dietary antioxidant index and metabolic dysfunction-associated steatotic liver disease in adults: a cross-sectional study from NHANES 2017–2020, Scientific Reports. 14 (2024) 13801. https://doi.org/10.1038/s41598-024-63965-1.

[38] M.-M. Li, Y.-T. Chen, J.-C. Ruan, et al., Structure-activity relationship of dietary flavonoids on pancreatic lipase, Current Research in Food Science. 6 (2023) 100424. https://doi.org/https://doi.org/10.1016/j.crfs.2022.100424.

[39] S. Alyar, T. Sen, Ü. Özmen, et al., Synthesis, spectroscopic characterizations, enzyme inhibition, molecular docking study and DFT calculations of new Schiff bases of sulfa drugs, Journal of Molecular Structure. 1185 (2019) 416-424. https://doi.org/10.1016/j.molstruc.2019.03.002.

[40] B. Sternby, D. Hartmann, B. BorgstroÖM, et al., Degree of in vivo inhibition of human gastric and pancreatic lipases by Orlistat (Tetrahydrolipstatin, THL) in the stomach and small intestine, Clinical Nutrition. 21 (2002) 395-402. https://doi.org/https://doi.org/10.1054/clnu.2002.0565.

[41] Y.S. Raouf, Covalent Inhibitors: To Infinity and Beyond, Journal of Medicinal Chemistry. 67 (2024) 10513-10516. https://doi.org/10.1021/acs.jmedchem.4c01308.

[42] Y. Yang, L. Lin, M. Zhao, et al., The hypoglycemic and hypolipemic potentials of Moringa oleifera leaf polysaccharide and polysaccharide-flavonoid complex, International Journal of Biological Macromolecules. 210 (2022) 518-529. https://doi.org/https://doi.org/10.1016/j.ijbiomac.2022.04.206.

[43] X. Shuai, T. Dai, D.J. McClements, et al., Hypolipidemic effects of macadamia oil are related to AMPK activation and oxidative stress relief: *In vitro* and *in vivo* studies, Food Research International. 168 (2023) 112772. https://doi.org/https://doi.org/10.1016/j.foodres.2023.112772.

[44] R.R. Kathak, A. Sumon, N.H. Molla, et al., The association between elevated lipid profile and liver enzymes: a study on Bangladeshi adults, Scientific Reports. 12 (2022) 1711. https://doi.org/10.1038/s41598-022-05766-y.

[45] X.X. Shuai, T.T. Dai, D.J. McClements, et al., Hypolipidemic effects of macadamia oil are related to AMPK activation and oxidative stress relief: *In vitro* and *in vivo* studies, Food Research International. 168 (2023) 112772. https://doi.org/10.1016/j.foodres.2023.112772.

[46] L.Y. Wei, H. Wu, X.F. Wang, et al., Comprehensive review of plant-derived anti-hyperlipidemia peptides: Production, anti-hyperlipidemia mechanism, and structure-activity relationship study, Food Chemistry. 461 (2024) 140715. https://doi.org/10.1016/j.foodchem.2024.140715.

[47] N. Chorhirankul, A.E.M. Janssen, R.M. Boom, UF fractionation of fish protein hydrolysate, Separation and Purification Technology. 330 (2024) 125232. https://doi.org/10.1016/j.seppur.2023.125232.

[48] I.M. Prados, M.L. Marina, M.C. García, Isolation and identification by high resolution liquid

chromatography tandem mass spectrometry of novel peptides with multifunctional lipid-lowering capacity, Food Research International. 111 (2018) 77-86. https://doi.org/https://doi.org/10.1016/j.foodres.2018.05.009.

[49] P. Wang, X. Song, Q. Liang, Molecular Docking Studies and In Vitro Activity of Pancreatic Lipase Inhibitors from Yak Milk Cheese, International Journal of Molecular Sciences. 26 (2025) 756. https://www.mdpi.com/1422-0067/26/2/756

[50] P. Wang, X. Song, Q. Liang, Study on the Inhibitory Effect of Bioactive Peptides Derived from Yak Milk Cheese on Cholesterol Esterase, Foods. 13 (2024) 2970. https://www.mdpi.com/2304-8158/13/18/2970

[51] I.M. Prados, J.M. Orellana, M.L. Marina, et al., Identification of Peptides Potentially Responsible for *In Vivo* Hypolipidemic Activity of a Hydrolysate from Olive Seeds, Journal of Agricultural and Food Chemistry. 68 (2020) 4237-4244. https://doi.org/10.1021/acs.jafc.0c01280.

[52] N. Xie, B. Wang, L. Jiang, et al., Hydrophobicity exerts different effects on bioavailability and stability of antioxidant peptide fractions from casein during simulated gastrointestinal digestion and Caco-2 cell absorption, Food Research International. 76 (2015) 518-526. https://doi.org/https://doi.org/10.1016/j.foodres.2015.06.025.

[53] L. Pinzi, G. Rastelli, Molecular Docking: Shifting Paradigms in Drug Discovery, International Journal of Molecular Sciences. 20 (2019) 4331. https://doi.org/10.3390/ijms20184331.

[54] L. Yang, S. Cao, M. Xie, et al., Virtual screening, activity evaluation, and stability of pancreatic lipase inhibitors in the gastrointestinal degradation of nattokinase, Heliyon. 10 (2024) e24868. https://doi.org/https://doi.org/10.1016/j.heliyon.2024.e24868.

[55] P. Zhang, L. Liu, Q. Huang, et al., Mechanism study on the improvement of egg white emulsifying characteristic by ultrasound synergized citral: Physicochemical properties molecular flexibility, protein structure, Ultrasonics Sonochemistry. 111 (2024) 107104. https://doi.org/10.1016/j.ultsonch.2024.107104.

[56] J.C. Zhang, J.C. Zhang, L. Liang, et al., Identification and virtual screening of novel umami peptides from chicken soup by molecular docking, Food Chemistry. 404 (2023) 134414. https://doi.org/10.1016/j.foodchem.2022.134414.

[57] H. Xiang, D.S. Waterhouse, P.Z. Liu, et al., Pancreatic lipase-inhibiting protein hydrolysate and peptides from seabuckthorn seed meal: Preparation optimization and inhibitory mechanism, Lwt-Food Science and Technology. 134 (2020) 109870. https://doi.org/10.1016/j.lwt.2020.109870.

[58] Z.W. Zhang, S.Q. Jiang, Y.Z. Li, et al., Residue profiles of peptides with cholesterol esterase and pancreatic lipase inhibitory activities through virtual screening and sequence analysis, Food Chemistry. 460 (2024) 140708. https://doi.org/10.1016/j.foodchem.2024.140708.

[59] Z.Q. Zhang, X.R. Ren, J. Geng, et al., Identification, characterization and hypolipidemic effect of novel peptides in protein hydrolysate from *Protaetia brevitarsis* larvae, Food Research International. 176 (2024) 113813. https://doi.org/10.1016/j.foodres.2023.113813.

[60] T. Robin, S. Reuveni, M. Urbakh, Single-molecule theory of enzymatic inhibition, Nature Communications. 9 (2018) 779. https://doi.org/10.1038/s41467-018-02995-6.

[61] A. Arsalan, H. Younus, Enzymes and nanoparticles: Modulation of enzymatic activity via nanoparticles, International Journal of Biological Macromolecules. 118 (2018) 1833-1847. https://doi.org/https://doi.org/10.1016/j.ijbiomac.2018.07.030.

[62] H. Yin, J.X. Zhu, Y. Zhong, et al., Kinetic and thermodynamic-based studies on the interaction mechanism of novel R. roxburghii seed peptides against pancreatic lipase and cholesterol esterase, Food Chemistry. 447 (2024) 139006. https://doi.org/10.1016/j.foodchem.2024.139006.

[63] X. Huang, J.X. Zhu, L. Wang, et al., Inhibitory mechanisms and interaction of tangeretin, 5-demethyltangeretin, nobiletin, and 5-demethylnobiletin from citrus peels on pancreatic lipase: Kinetics, spectroscopies, and molecular dynamics simulation, International Journal of Biological Macromolecules. 164 (2020) 1927-1938. https://doi.org/10.1016/j.ijbiomac.2020.07.305.

[64] H. Wu, W. Zeng, L. Chen, et al., Integrated multi-spectroscopic and molecular docking techniques to probe the interaction mechanism between maltase and 1-deoxynojirimycin, an α-glucosidase inhibitor, International Journal of Biological Macromolecules. 114 (2018) 1194-1202. https://doi.org/https://doi.org/10.1016/j.ijbiomac.2018.04.024.

[65] Q.Z. Liu, H. Zhang, H.Q. Dai, et al., Inhibition of starch digestion: The role of hydrophobic domain of both α-amylase and substrates, Food Chemistry. 341 (2021) 128211. https://doi.org/10.1016/j.foodchem.2020.128211.

[66] H.F. Yu, S.Z. Dong, L.Y. Wang, et al., The effect of triterpenoid saponins on pancreatic lipase *in vitro*: Activity, conformation, kinetics, thermodynamics and morphology, Biochemical Engineering Journal. 125 (2017) 1-9. https://doi.org/10.1016/j.bej.2017.05.010.

[67] S. Sinha, B. Tam, S.M. Wang, Applications of Molecular Dynamics Simulation in Protein Study, Membranes. 12 (2022) 844. https://www.mdpi.com/2077-0375/12/9/844

[68] T. Gao, R. Yan, N. Fang, et al., Alisol C 23-acetate might be a lead compound of potential lipase inhibitor from *Alismatis Rhizoma*: Screening, identification and molecular dynamics simulation, International Journal of Biological Macromolecules. 278 (2024) 134878. https://doi.org/10.1016/j.ijbiomac.2024.134878.

[69] H. Yin, J. Zhu, Y. Zhong, et al., Kinetic and thermodynamic-based studies on the interaction mechanism of novel R. roxburghii seed peptides against pancreatic lipase and cholesterol esterase, Food Chemistry. 447 (2024) 139006. https://doi.org/https://doi.org/10.1016/j.foodchem.2024.139006.

[70] M. Wu, M. Liu, F.Y. Wang, et al., The inhibition mechanism of polyphenols from *Phyllanthus emblica* Linn. fruit on acetylcholinesterase: A interaction, kinetic, spectroscopic, and molecular simulation study, Food Research International. 158 (2022) 111497. https://doi.org/10.1016/j.foodres.2022.111497.

[71] X. Li, Y. Pu, H. Jiang, et al., Inhibitory effect of procyanidin B2 and tannin acid on cholesterol esterase and their synergistic effect with orlistat, Food Science and Human Wellness. 13 (2024) 360-369. https://doi.org/10.26599/FSHW.2022.9250030.

[72] P.T. Nguyen, H.A. Huynh, D.V. Truong, et al. Exploring Aurone Derivatives as Potential Human

Pancreatic Lipase Inhibitors through Molecular Docking and Molecular Dynamics Simulations. *Molecules.* 25. 2020.

[73] J.K. Pan, M. Nawaz, J.C. Liu, et al., Exploring synergistic inhibitory mechanisms of flavonoid mixtures on α-glucosidase by experimental analysis and molecular dynamics simulation, Food Chemistry. 464 (2025) 141560. https://doi.org/10.1016/j.foodchem.2024.141560.

[74] Z.K. Li, W.H. Zhang, M.A. Abubaker, et al., In silico identification and experimental validation of two types of angiotensin-converting enzyme (ACE) and xanthine oxidase (XO) milk inhibitory peptides, Food Chemistry. 464 (2025) 141864. https://doi.org/10.1016/j.foodchem.2024.141864.

[75] X. Zhang, W. Li, Y. Tang, et al., Mechanism of Pentagalloyl Glucose in Alleviating Fat Accumulation in Caenorhabditis elegans, Journal of Agricultural and Food Chemistry. 67 (2019) 14110-14120. https://doi.org/10.1021/acs.jafc.9b06167.

[76] K.Q. Xu, J.F. Dou, C.E. Wu, et al., Effects of ultrasound-assisted Fenton treatment on structure and hypolipidemic activity of apricot polysaccharides, Food Bioscience. 50 (2022) 102073. https://doi.org/10.1016/j.fbio.2022.102073.

[77] Z. Liu, L. Cheng, B. Yang, et al., Effects of moderate static magnetic fields on the lipogenesis and lipolysis in different genders of Caenorhabditis elegans, Ecotoxicology and Environmental Safety. 259 (2023) 115005. https://doi.org/https://doi.org/10.1016/j.ecoenv.2023.115005.

[78] P.Y. Shen, J.C. Kershaw, Y.R. Yue, et al., Effects of conjugated linoleic acid (CLA) on fat accumulation, activity, and proteomics analysis in *Caenorhabditis elegans*, Food Chemistry. 249 (2018) 193-201. https://doi.org/10.1016/j.foodchem.2018.01.017.